ISSUE 3 | FEBRUARY 2016

TTA E-Magazine

TRIBOLOGY RESOURCES FOR INDUSTRIAL PROFESSIONALS

ICTMP 2016

การประชุมวิชาการนานาชาติ ICTMP 2016

Machine Reliability Seminar

การสัมมนาเกี่ยวกับความน่าเชื่อถือของเครื่องจักร

Tribology in Malaysia

ไทรโบโลยีในประเทศมาเลเซีย

THAI TRIBOLOGY ASSOCIATION (TTA)

CONTENT

TTA President's Message

สารจากนายกสมาคมการสึกหรอและการหล่อลื่นไทย

Assoc.Prof. Siriluck Vinitchanyong (President of Thai Tribology Association)

รศ. ศิริลักษณ์ นิวิฐจรรยงค์ (นายกสมาคมการสึกหรอและการหล่อลื่นไทย)

After Thai Tribology Association (TTA) was officialy established, we have had many interests from many foreign tribologists and organizations who would like to publish their works in TTA E-Magazine. On behalf of TTA working group committee, we are truly appreciated all the submitted articles. They are all very interesting and definitely worth reading. In the 3rd issue of TTA E-Magazine, some of the selected articles will be presented and I really hope that the readers will find these articles beneficial to their works.

In addition, TTA will organize two tribology events this year: ICTMP 2016 and a seminar in MHE'16. More information can be found in the articles. I also would like to invite you to participate in these great events and hope to see you there.

หลังจากที่สมาคมการสึกหรอและการหล่อลื่นไทย (TTA) ได้ก่อตั้งอย่างเป็นทางการมาไม่นาน ทางสมาคมก็ได้รับการติดต่อจากนักวิจัยและองค์กรทางด้านไทรโบโลยีจากต่างประเทศเพื่อที่จะนำเสนอผลงานใน TTA E-Magazine ในฐานะตัวแทนของคณะทำงานของ TTA ทางสมาคมรู้สึกซาบซึ้งเป็นอย่างยิ่งจากการได้รับบทความจากต่างประเทศ ซึ่งบทความทั้งหมดนั้นน่าสนใจและคุ้มค่ากับการได้อ่านเป็นอย่างยิ่ง ใน TTA E-Magazine ฉบับที่ 3 นี้ จะมีบทความที่ได้ถูกคัดเลือกมาจากต่างประเทศมานำเสนอ และดิฉันหวังเป็นอย่างยิ่งว่าผู้อ่านจะได้รับประโยชน์จากบทความที่นำเสนอ

นอกจากนี้แล้วทางสมาคมกำลังจะมีการจัดงานทางด้านไทรโบโลยีสองงานคือ ICTMP 2016 และ การจัดสัมมนาในงาน MHE'16 ดิฉันอยากจะขอเชิญชวนให้ผู้อ่านเข้าร่วมงานและหวังว่าคงจะได้มีโอกาสเจอท่านในงานไทรโบโลยีทั้งสองนี้

Thai Parkerizing Co., Ltd.

THAI PARKERIZING CO., LTD.

Thai Parkerizing is a leader in Surface Treatment and Heat Treatment industry. We focus in best Quality and Technology development to utilize our products and service to fulfill our customer satisfaction.

THAI PARKERIZING

We provide variety of products and service to apply on each metal surface such as iron and steel, gavanized steel, aluminum i.e. Our products are applied to many customer processes since metal upstream toward OEM (Original Equipment Manufacturer) finish goods.

CHEMICAL PRODUCTS

Conversion coating chemicals

- Zinc phosphate coating
- Zinc calcium phosphate coating
- Manganese phosphate coating
- Metal oxide coating
- Trivalent chrome coating
- Non-chrome coating
- Stearate soap coating
- Dry-in-place lubricant coating (PULS)

Rust preventive products

Depend on your requirement for rust protection

- Solvent base type
- Wax base type
- Water base type
- PIPAK (Volatile Corrosion Inhibitor Film)

Rolling oil

Applied as coolant for cold rolled steel process

- Lubricity
- High rolling speed

Other treatment products

- Degreasing and cleaning chemicals
- Hydrophilic coating on evaporator
- Coil coating on galvanized steel (Chromate free)
- Short-term rust preventive chemicals
- Paint remover

THAI PARKERIZING CO., LTD.


Solar cell


Auto rack


Container lifting robot


Automatic production system

TREATMENT SERVICE

Surface treatment

Phosphate treatment

- Zinc phosphate coating
- Manganese phosphate coating
- Aluminum treatment
- Trivalent chrome coating
- Zinc phosphate and soap lubricant

Pallube treatment
(Solid lubrication treatment)

- Molybdenum disulfide (MoS_2)
- Teflon (PTFE)

Kanigen®
(Nikel electroless plating)

- Ni-P alloy coating
- Ni-P-B alloy coating
- Ni coating with PTFE
- Ni-Co-W-P alloy coating

DELTA-MKS®

- Zinc aluminium flakes
- Small coating thickness (5-20μm)
- Cathodic corrosion protection
- No hydrogen embrittlement

Heat treatment

Gas heat treatment

- Gas carburizing
- Gas carbonitriding
- Gas soft nitriding
- Quenching and tempering

ISONITE®
(Salt Bath Soft Nitriding)

- Quench-Polish-Quench
- Surface hardness/ Wear resistance
- Corrosion resistance

Shot peening

- Fatigue strength
- Modify metal surface

PVD
(Physical Vapor Deposition)

- TiN
- TiC
- CrN
- TiAlN
- DLC (Diamond Like Carbon)

SERVICE LABORATORY

Surface and metallurgical analysis

- Microstructure and chemical composition
- Mapping and depth profile analysis
- Wear and friction test
- Corrosion test and paint evaluation

Environment analysis

- Hazardous substance analysis (Pb, Cd and Cr^{6+})
- Waste water analysis (pH, BOD, COD, TDS, SS, Heavy metal, Oil & Grease and Cyanide)

Chemical analysis

- Organic and inorganic analysis
- Qualitative and quantitative analysis

Zinc phosphate standard panel

- Verify corrosion and paint evaluation

Tribology in Malaysia: General Perspective

ไทรโบโลยีในประเทศมาเลเซีย: มุมมองทั่วไป

Written by M.F.B. Abdollah (Universiti Teknikal Malaysia Melaka), S. Kasolang (Universiti Teknologi MARA), N.W.M. Zulkifli (University of Malaya), M.J. Ghazali (Universiti Kebangsaan Malaysia), I.C. Gabeshuber (Vienna University of Technology) and H.H. Masjuki (University of Malaya)






INTRODUCTION

Tribology was first coined in 1966 as documented in 'Jost Report'. The word 'tribology' has since gained a common usage for matters related to friction, wear, and lubrication in machine interactions. Since tribology is an engineering issue that goes beyond national boundaries, many tribology societies have emerged across the continents partly motivated by the pursuit for greener world via waste reduction. The move for improved tribology practices in industry has reached Malaysia and in 2007, Malaysian Tribology Society (MYTRIBOS) was established by local tribologists [1]. MYTRIBOS is responsible to promote proper practices in research and development related to the field of tribology in Malaysia and to facilitate collaborations between academia and industry in all possible endeavors. MYTRIBOS eventual vision and mission is to help reduce energy consumption by making machineries more energy efficient in order to reduce greenhouse gas emission. MYTRIBOS is contributing towards the improvement of the environment and to achieve a better quality of life and more sustainable world by creating awareness of the importance of practicing proper tribology. From a humble beginning in 2007, MYTRIBOS now can be proud of its current progress with 89 registered members, coming from different background and areas of interests, from local and international universities, industries and research institutes. Specifically, more than 80% of MYTRIBOS members are locals and the rest are expatriates working in Malaysia. The organizational structure of MYTRIBOS for the period of 2013 to 2015 is shown in Figure 1.

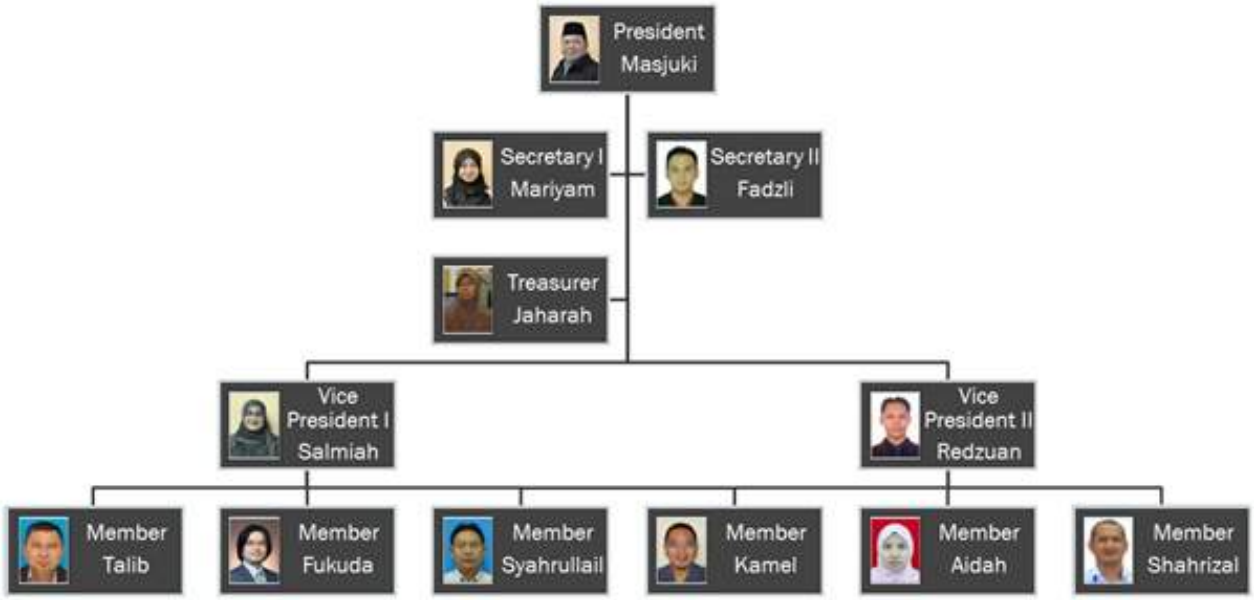

Figure 1. MYTRIBOS executive committee (2013-2015).

CURRENT TRIBOLOGY RESEARCH TRENDS IN MALAYSIA

The current tribology research trends in Malaysia can be classified into five main categories: (a) Green Tribology (b) Hydrodynamic lubrication in plain journal bearing (c) Tribology of waste materials (d) Surface and coatings technology, and (e) Biomimetics.

Green tribology involves research and development of bio-based lubricants, pioneered by Masjuki and his co-workers at University of Malaya in the early 1980's. In relatively recent years, the work by Zulkifli et al. [2] examined the lubricity of bio-based lubricant derived from different chemically modified fatty acid methyl ester. This bio based lubricant was synthesized using palm oil methyl ester, pentaerythritol, and trimethylolpropane. They have also investigated the effect of bio-based lubricant on coating and surface modification. In another group, Belinda and her co-worker work on improved friction and wear performance of micro-dimpled ceramic-on- ceramic interface for hip joint [3].

Many aspects of research work specifically in hydrodynamic lubrication of plain journal bearing have been published by Kasolang et al. [4] who started their work at the University of Sheffield. The work that started at the University of Sheffield has been further established at the Universiti Teknologi MARA through co-supervisions of postgraduate students between the two universities. One of the early highlights of the investigation is on the use of reflection measurement technique to measure film thickness and viscosity around the circumference of the journal bearing. In later work, other response parameters such as friction, temperature profile, and pressure profile were also reported. Kasolang and co-workers [5-6] have started working on other aspects of tribology namely wear and bio lubricants.

Nowadays, the need for engineering materials to be environmentally friendly is rising. Waste materials may be considered a secondary source of materials with an energetic advantage due to its high energy content. With regard to this research area, Abdollah and his co-workers strive at seeking innovative and sustainable solutions to these questions by developing a new potential self-lubricating and friction materials made from agriculture wastes [7-10]. This effort by young researchers from Universiti Teknikal Malaysia Melaka is expected to have large potential

for advancing a zero waste strategy in improving tribological properties at an affordable cost.

Surface treatments including coatings are rapidly developing areas in tribology that offer new methods and techniques to control friction and wear. In a series of research collaborations between researchers from Universiti Kebangsaan Malaysia and SIRIM Berhad resulted in more than a half dozen top-tier research publications since 2013. Ghazali and her co-workers have been working on oxide-ceramic materials for marine environments, particularly for tropical countries to mitigate corrosion and wear [11-14]. Identification on vital parameters in plasma sprayed coating including good surface textures had improved the quality of depositions and coatings on the substrates for severe conditions, in particular.

Gebeshuber is an Austrian Professor of Physics who has been living and working in Malaysia since 2009. As a nanotechnologist, she is well aware of the importance of the nanoscale in tribological applications, and her work bridges across scales, from nano to the device level. She has been working on bioinspired MEMS on diatom tribology and on green nanotribology. She introduces biology for tribologists and highlighted the benefits of biomimetics in her latest publication [15].

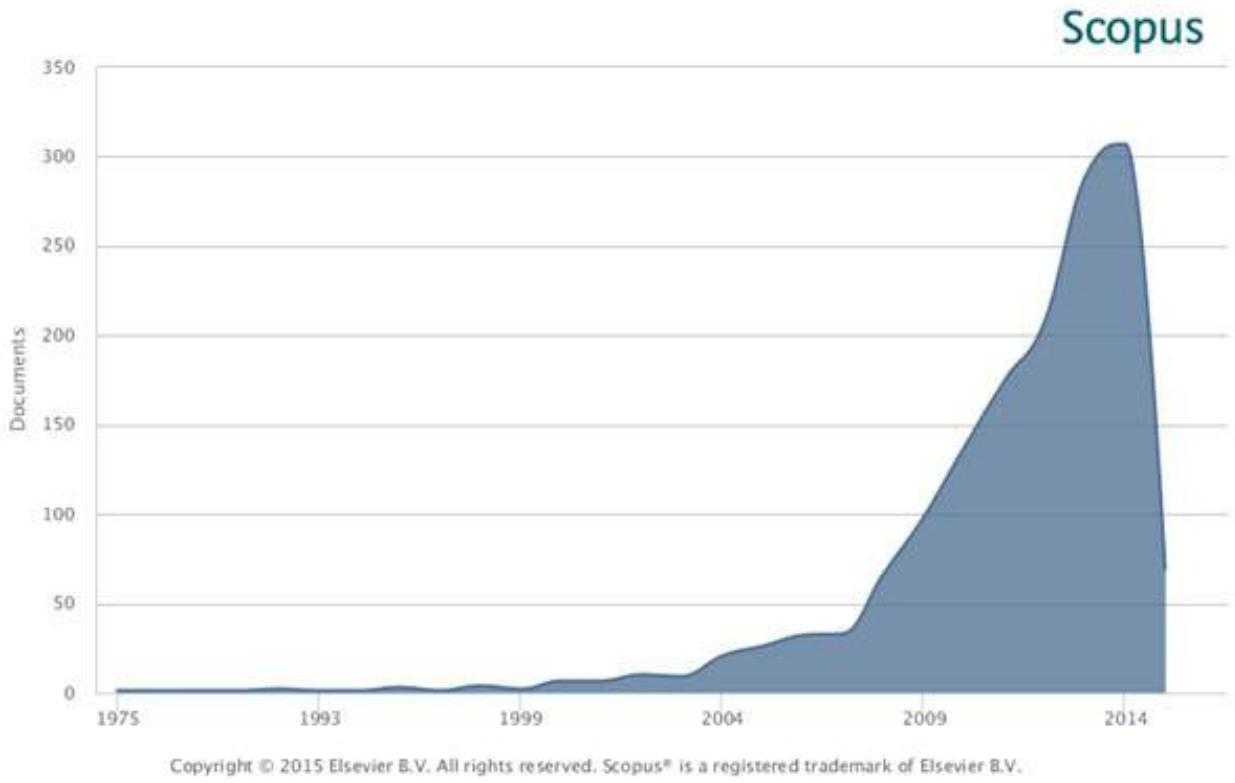

Figure 2. Number of papers affiliated to Malaysia, which fall in the field of tribology and published in Scopus database. The keywords used are tribology, wear, friction, lubrication [16].

MALAYSIAN PUBLICATION IN THE FIELD OF TRIBOLOGY

The publication record of various research organizations and academic organizations were tracked down from as early as 1975 to the current year 2015 and the publication profile obtained is given in Figure 2. The data shown in Figure 2 was based on Scopus database [16]. Scopus has practically made data searching and compilation on tribology progress in Malaysia easy which otherwise can be a daunting task to accomplish. Based on the number of published pa-

pers, it is uplifting to note that the intensity of research in tribology in Malaysia has increased tremendously since 2007, the year MYTRIBOS was born. It is worth noting that one of the MYTRIBOS objectives, to promote Malaysia in the field of tribology through publications, has been progressively achieved.

MYTRIBOS has moved one step further with the establishment of Jurnal Tribologi making its debut in 2014 [17]. Jurnal Tribologi is strategically written in Malay to signify local efforts but with global impact. This journal is an open access of peer-reviewed international journal, dedicated to the rapid publication of high quality papers on important subjects in the areas of tribology and other emerging fields related to friction, wear and lubrication. MYTRIBOS also regularly organizes international conferences and this year, Malaysian International Tribology Conference (MITC2015) will be held in Penang [18]. The presence of MYTRIBOS has been recognized and appreciated internationally with the recent appointment as the host of the coming ASIATRIB in 2018. Indeed, MYTRIBOS is committed and all geared for promoting the advancement of tribology in Malaysia as well as abroad in support of a more sustainable world.

TRIBOLOGY RELATED INDUSTRY

Tribology related industry may be defined as those companies that engage with friction, wear, and lubrication related products and technology. The role of industry in promoting tribology is tremendous. In Malaysia, this has yet to grow and MYTRIBOS has a major role to play. In the context of Malaysia, PETRONAS, as a strong local industry with global presence in more than 23 countries, is a force to reckon with. In downstream business, PETRONAS helps to enhance Malaysia's oil and gas resources. PETRONAS has a total refining capacity of 500,000 barrels per day and one of key petroleum products produced is lubricants. A subsidiary company known as PETRONAS Lubricants International Sdn. Bhd. (PLI) was established in 2008 to cater for lubricants global demand. Currently, some of the lubricants based products produced by PETRONAS include PETRONAS Syntium, PETRONAS Sprinta, and PETRONAS Urania for passenger vehicles, motorcycles, and commercial vehicles respectively. The commitment of PETRONAS in supporting national education agenda is evident from its engagements with education providers. Universiti Teknologi PETRONAS (UTP) and PETROSAINS are the mark of its commitment. In the case of Universiti Teknologi MARA, PETRONAS has also established collaborations with different faculties such as the Faculty of Mechanical Engineering and Faculty of Chemical Engineering. PETRONAS's engagement with universities come in different forms including research, industrial placement, training, and sponsorship [19]. Indeed PETRONAS is a pride of Malaysia in so many ways.

The roles of PETRONAS are also championed and complimented by other companies such as HYRAX Oil [20], Baseron (M) Sdn. Bhd., VICSON Sdn. Bhd., MEGA Energy Sdn. Bhd, HAKITA Engineering Sdn. Bhd., ZETA Scientific Sdn. Bhd., Lubeworld Holdings Sdn. Bhd., CBM Solutions Sdn. Bhd., Sumber Petroleum Cemerlang Sdn. Bhd., Tenaga Nasional Berhad, QES (Asia Pacific) Sdn. Bhd., PROEIGHT Sdn. Bhd., TOYO Grease Sdn. Bhd., SYNTOMAX Industries Sdn. Bhd., and FEOSO Group [21].

REFERENCES

[1] www.mytribos.org

[2] N.W.M. Zulkifli, S.S.N. Azman, M.A. Kalam, H.H. Masjuki, R. Yunus, M. Gulzar, Lubricity of bio-based lubricant derived from different chemically modified fatty acid methyl ester, Tribology International (2015), In press. doi:10.1016/j.triboint.2015.03.024.

[3] T. Roy, D. Choudhury, S. Ghosh, A. Bin Mamat, B. Pingguan-Murphy, Improved friction and wear performance of micro dimpled ceramic-on-ceramic interface for hip joint arthroplasty, Ceramic International, 41 (2015) 681-90.

[4] S. Kasolang, D.I. Ahmed, R.S. Dwyer-Joyce, B. F. Yousif, Performance analysis of journal bearings using ultrasonic reflection, Tribology International, 64 (2013) 78-84.

[5] S. Kasolang, M.A. Ahmad, M.A.A. Bakar, A.H.A. Hamid, Specific wear rate of kenaf epoxy composite and oil palm empty fruit bunch (OPEFB) epoxy composite in dry sliding, Jurnal Teknologi (Science and Engineering), 58 (2012) 85—88.

[6] D.I. Ahmed, S. Kasolang, R.S. Dwyer-Joyce, K.I. Sainan, N.R. Nik Roselina, Formulation and physico-chemical characteristics of biolubricant, Jurnal Tribologi, 3 (2014) 1-10.

[7] A. Mustafa, M.F.B. Abdollah, N. Ismail, H. Amiruddin, N. Umehara, Materials selection for eco-aware lightweight friction material, Mechanics & Industry, 15 (2014) 279-285.

[8] K.W. Chua, M.F.B. Abdollah, N. Ismail, H. Amiruddin, Potential of palm kernel activated carbon epoxy (PKAC-E) composite as solid lubricant: Effect of load on friction and wear properties. Jurnal Tribologi, 2 (2014) 31-38.

[9] A. Mustafa, M.F.B. Abdollah, N. Ismail, H. Amiruddin, N. Umehara, Selection and verification of kenaf fibres as an alternative friction material using weighted decision matrix method, Materials & Design, 67 (2015) 577-582.

[10] N.A. Mat Tahir, M.F.B. Abdollah, R. Hasan, H. Amiruddin, The effect of temperature on the tribological properties of palm kernel activated carbon-epoxy composite, Tribology Online, In press.

[11] N.H.N. Yusoff, M.J. Ghazali, M.C. Isa, A.R. Daud, A. Muchtar, Effects of powder size and metallic bonding layer on corrosion behaviour of plasma-sprayed Al2O3-13% TiO2 coated mild steel in fresh tropical seawater, Ceramic International, 39 (2013) 2527-2533.

[12] S.M. Forghani, M.J. Ghazali, A. Muchtar, A.R. Daud, N.H.N. Yusoff, C.H. Azhari, Effects of plasma spray parameters on TiO2-coated mild steel using design of experiment (DoE) approach, Ceramic International, 39 (2013) 3121-3127.

[13] S.M. Forghani, M.J. Ghazali, A. Muchtar, A.R. Daud, Mechanical properties of plasma sprayed nanostructured TiO2 coatings on mild steel, Ceramic International, 40 (2014) 7049-7056.

[14] M.J. Ghazali, S.M. Forghani, N. Hassanuddin, A. Muchtar, A.R. Daud, Comparative wear study of plasma sprayed TiO2 and Al2O3—TiO2 on mild steels, Tribology International, (2015), In press. doi:10.1016/j.triboint.2015.05.001

[15] I.C. Gebeshuber, Biomimetic inspiration regarding nano-tribology and materials issues in MEMS, in: S.J. Sinha, N. Satyanarayana, S.C. Lim (Eds.), Nano-tribology and Materials in MEMS, Springer, 2013, pp. 53-79.

[16] www.scopus.com

[17] http://jurnaltribologi.mytribos.org

[18] http://mitc2015.mytribos.org

[19] www.petronas.com.my

[20] www.hyraxoil.com

[21] www.feoso.group

akebono

BRAKE EXPERTS

Study of Liquid-Mediated Adhesion between 3D Rough Surfaces: A Spectral Approach

การศึกษาเกี่ยวกับ Liquid-Mediated Adhesion ระหว่างพื้นผิวขรุขระในรูปแบบสามมิติ: วิธี Spectral

Amir Rostami* (Corresponding Author, Email: amir.rostami@gatech.edu, Phone: 334-524-5942)

Jeffrey L. Streator*

*G. W. Woodruff School of Mechanical Engineering, Georgia Institute of Technology, Atlanta, GA 30332-0405, USA

Abstract

In this work, a three-dimensional model for liquid-mediated adhesion between two rough surfaces is presented. The approach is based on a spectral (multi-scale) representation of compressive rough surface deformation along with the capillary equations governing the tensile deformation. An iterative numerical algorithm is designed to solve the equations of elasticity and capillarity simultaneously. It is shown that, under certain conditions, a contact instability occurs leading to unbounded rates of change of tensile force, average gap and wetted radius. The effects of liquid volume, liquid surface tension, surface topography, nominal contact area, and external load on the stability of contact interface are studied. Key dimensionless ratios are identified that govern the equilibrium state and onset of instability.

Keywords: Liquid-mediated adhesion, Surface roughness, Multi-scale, Collapse, Capillary.

Nomenclature

A	contact area of a sinusoidal asperity
$(A_{JGH})_1$	contact area at early contact of sinusoidal asperity per JGH model [1]
$(A_{JGH})_2$	contact area at near complete contact of sinusoidal asperity per JGH model [1]
A_n	nominal contact area between two rough surfaces
A_r	real contact area between two rough surfaces
A_w	area of wetted region
B	aspect ratio (ratio of sinusoidal asperity amplitude to its wavelength)
β	equivalent 1D Fourier coefficient
Δ	amplitude of sinusoidal asperity
Δg_k	reduction in the average surface separation at frequency scale k
Δp	capillary pressure drop
ΔV_c	volume loss due to compressive stresses
ΔV_t	volume loss due to tensile stresses
ΔV_{tot}	total volume loss
E	elastic modulus
E'	reduced or effective elastic modulus
$E(k)$	elliptical integral of the second kind
η	areal density of asperities
f	spatial frequency (reciprocal of wavelength)
F	total force between two rough surfaces
F_c	compressive force between rough surfaces
F_t	tensile force between rough surfaces
F_t^*	non-dimensional tensile force
$F(k_x, k_y)$	2D FFT coefficients
g	local surface separation for a single asperity
$\overline{g}$	average surface separation for a single asperity
γ	surface tension of liquid
Γ	non-dimensional adhesion parameter
h_{fs}	surface separation at the free surface of the liquid
$\overline{h}$	average surface separation
$k_{x,y}$	indices correspond to spatial frequencies in x and y directions
$\overline{\kappa}$	mean curvature at the free surface of liquid
$\kappa_{I,II}$	principal curvatures at the free surface of the liquid
l_c	correlation length
$L_{x,y}$	scan lengths in x and y directions
λ	wavelength of sinusoidal asperity
$n_{x,y}$	indices correspond to spatial coordinate in x and y directions
$N_{x,y}$	number of nodal points in x and y directions
υ	Poisson's ratio
$\overline{p}$	average contact pressure of a sinusoidal asperity
p^*	average contact pressure for complete contact of a sinusoidal asperity
P	external load applied to rough surfaces
P^*	non-dimensional external load
r	radial coordinate
r_w	radius of wetted region
$R_{I,II}$	principal radii of curvature at the free surface of the liquid
σ	root mean square of rough surface heights
$\theta_{A,B}$	contact angles between the liquid and rough surfaces
$u_t(r)$	surface deformation due to tensile force
V_0	liquid volume
V_0^*	non-dimensional liquid volume
$z(x,y)$	rough surface heights
z_{max}	maximum value of the surface heights

1. Introduction

Significant attention has been given to liquid-mediated adhesion between solid surfaces in recent years due to its influence in micro/nano-scale devices [2-7]. Small spacing between solid surfaces and high surface area to volume ratio make the surface-driven forces such as adhesion important in small-scale devices such as micro/nano-electro-mechanical systems (MEMS/NEMS), head-disk interface (HDI), and the tip of atomic force microscope (AFM). The presence of a wetting liquid between solid surfaces causes adhesion which negatively affects the performance of these devices. The wetting liquid present in the interface due to condensation, contamination, or lubrication produces large concave meniscus curvatures at the liquid-vapor interface which induces large negative pressures. In fact Yang et al. [8], based on experiments with an AFM tip, concluded that the pressure can be negative down to -160 MPa.

Several authors have developed models to describe the behavior of solid-solid contact in the presence of a liquid film [9-20]. These works can be divided into two categories: (1) liquid-mediated adhesion between smooth surfaces [9-12], and (2) liquid-mediated adhesion between rough surfaces [13-20]. Matthewson and Mamin [9] modeled the liquid film adhesion between two ultra-flat solid surfaces where different regimes were identified by differing the quantities of liquid between the surfaces. Matthewson [13] also modeled the liquid-mediated adhesion between two rough spheres concentrating on the viscous component of adhesion. Poon and Bhushan [14], and Tian and Bhushan [15] presented a numerical contact model for the contact between three-dimensional rough surfaces in the presence of a liquid film. In their model, liquid-mediated adhesion arises from many isolated capillary bridges in the contact interface. The stiction phenomenon is investigated and results are obtained for the meniscus force versus the topographical properties of the rough surfaces. Their work is relevant for films of liquid thinner than considered in the current work. Persson [17] studied the effect of relative humidity on the work of adhesion and the contact area between two elastic solids with randomly rough surfaces. Streator and Jackson [18], and Streator [19] used spectral and deterministic approaches, respectively, to model the contact between 2D elastic rough surfaces in the presence of a liquid film. The tensile force between the surfaces due to liquid-mediated adhesion is calculated and a "surface collapse" phenomenon is observed in their work which corresponds to a sudden jump in the tensile force between the surfaces.

In the current work, a model for the liquid-mediated adhesion between three-dimensional (3D) rough surfaces is presented using a multi-scale contact model developed by Jackson and Streator [21] (from here on referred to as the JS model). The JS model is

based on representing contact between surfaces in multiple scales of roughness based on Fourier series coefficients. This work represents an extension of previous work on the liquid-mediated adhesion between 2D rough surfaces [18], as well as an extension of preliminary work done by the authors on liquid-mediated adhesion between 3D rough surfaces [22].

2. Contact Model

Figure 1 shows, schematically, the interface of interest. It consists of a rough surface with nominal contact area having side length L in x and y directions ($A_n = L^2$) and with surface heights in z direction. A rigid flat surface (which is shown as transparent in Fig. 1) with the same nominal contact area deforms the rough surface in the presence of a liquid film bridging between the two surfaces. It should be noted that the combination of a rigid flat and a rough surface used in this work is a model of two hypothetical elastic rough surfaces, whereby the rough surface of the model is given the combined roughness and flexibility of the hypothetical surface pair. It is well-known that if the liquid wets the two surfaces, a sub-ambient pressure will be developed within the liquid bridge which induces tensile (adhesive) stresses between the two surfaces [23]. This pressure drop depends on the curvature at the free surface of the liquid film, and the curvature, in turn is inversely proportional to the local spacing at the free surface of the liquid film. The thinner is the local gap, the greater is the pull effect between the two surfaces. As the surfaces are pulled together and the gap between them decreases, the more the liquid tends to pull them together. As the surfaces are brought into closer proximity, the compressive stresses begin to rise at the points of contact. There are two potential scenarios [18, 19]: (1) the tensile and compressive forces come into balance with an average gap in the order of composite surface roughness, or (2) the tensile force dominates the compressive force, and the interface collapses such that the average gap is a very small fraction of composite surface roughness. In the current work, the goal is to predict the equilibrium configuration for the contact of 3D rough surfaces in the presence of liquid film given the surface topography, elastic properties, liquid volume, liquid surface tension, and external load.

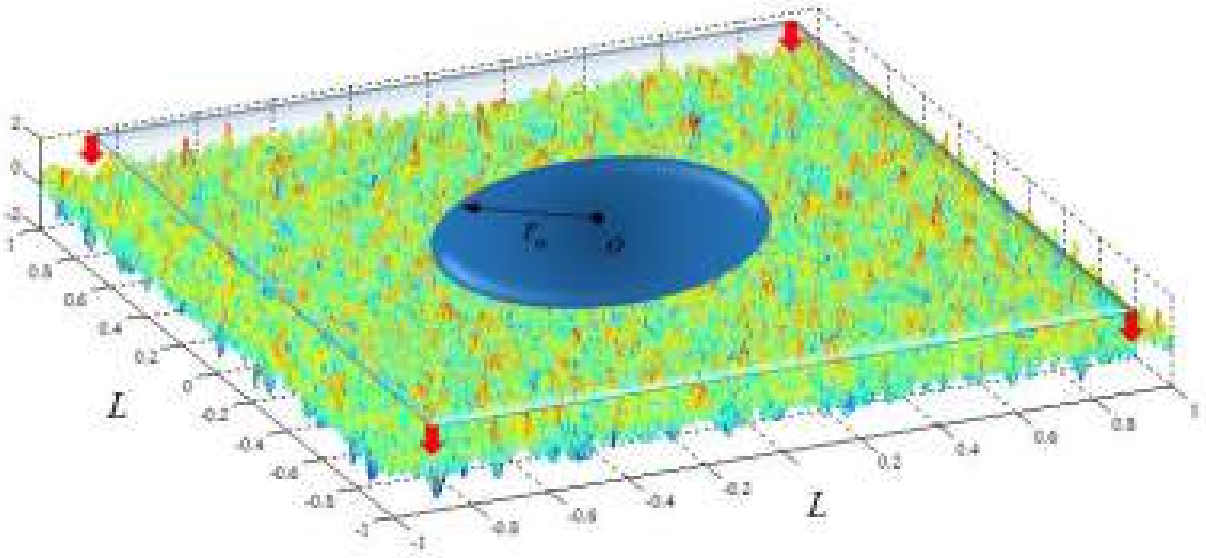

Figure 1. Schematic depiction of the contact interface: contact of a rigid flat surface and a simulated 3D elastic rough surface in presence of a liquid film

2.1 Tensile Stresses

As previously mentioned, a wetting liquid induces a pressure drop across the free surface. This pressure drop can be obtained based on the Laplace-Young equation (e.g. [23])

$$\Delta p = \gamma\left(\frac{1}{R_I}+\frac{1}{R_{II}}\right)=\gamma\left(\kappa_I+\kappa_{II}\right)=2\gamma\bar{\kappa} \qquad (1)$$

where Δp is the pressure drop across the interface of the liquid, γ is the liquid film surface tension, $R_{I,II}$ are the principal radii of curvature at the free surface of the liquid, $\kappa_{I,II}$ are the principal curvatures, and $\bar{\kappa}$ is the mean curvature at the free surface of the liquid. In this work, the effect of gravity is neglected and, due to assumed continuity, the liquid film is in hydrostatic equilibrium with uniform pressure throughout. Hence, according to Eq. (1), the curvature is the same at any point at the free surface of the liquid. Thus, the free surface of the liquid at any cross section cutting along the diameter of the liquid film is a part of a circle (Fig. 2).

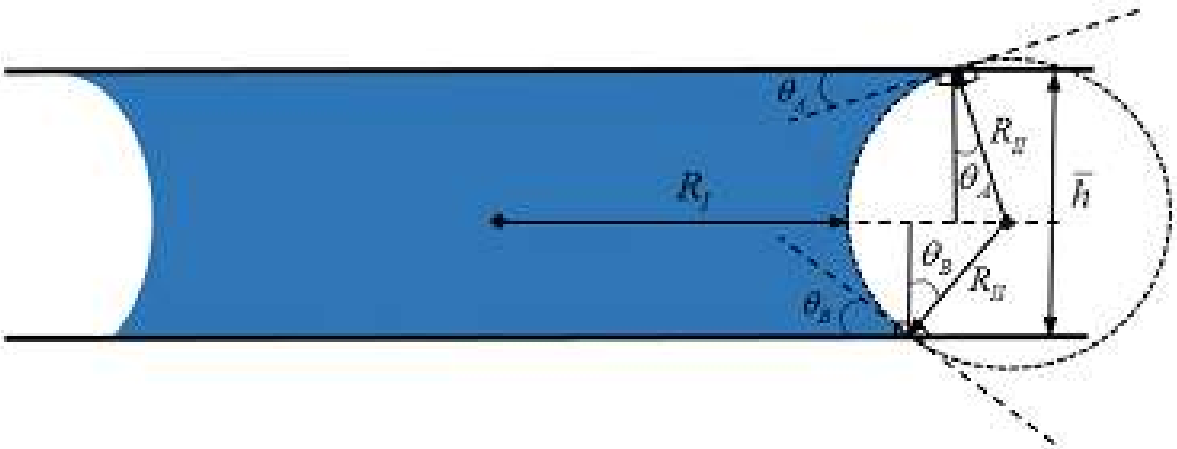

Figure 2. The free surface of the liquid along with radii of curvature and the average gap between the surfaces

According to Fig.2, setting $R_I = r_w$ and $R_{II} = R$ in Eq.(1) we have

$$\Delta p = \gamma\left(\frac{1}{R} + \frac{1}{r_w}\right) \tag{2}$$

The assumption $R << r_w$ seems reasonable since the gap between the contacting surfaces at the free surface, h_{fs}, is very small (in the order of microns), and this causes R to be small compared to the radius of wetted area, r_w. Thus, we have

$$\Delta p = \frac{\gamma}{R} \tag{3}$$

The radius of curvature at the free surface, R, can be related to the gap at the free surface, h_{fs}, by

$$h_{fs} = R(\cos\theta_A + \cos\theta_B) \tag{4}$$

where $\theta_{A,B}$ are the contact angles of the liquid film with lower and upper surfaces, respectively. Now, replacing for R from Eq.(4) in (3), the following relation between the pressure drop and the gap at the free surface can be obtained

$$\Delta p = \frac{\gamma}{h_{fs}}(\cos\theta_A + \cos\theta_B) \tag{5}$$

The average gap, $\overline{h}$, will be used in the current work to calculate the pressure drop, which is average gap between the two rough surfaces in the wetted region, replacing the gap at the free surface, h_{fs}. Working with $\overline{h}$ as in Eq.(6), simplifies the numerical process needed to arrive at a converged solution.

$$\Delta p = \frac{\gamma}{\overline{h}}(\cos\theta_A + \cos\theta_R) \quad (6)$$

The pressure drop calculated by Eq. (6) induces tensile stresses on each surface wherever the liquid film is present. Opposing these tensile stresses are the compressive stresses that are developed at the solid-solid contact points, which prevent the reduction in spacing between the two contacting surfaces. As the average gap between the two surfaces reduces, the liquid will expand over a larger area between the two surfaces, and it will also have a higher pressure drop due to the reduction in the gap. Hence, two possibilities can occur in the battle between the tensile and compressive forces. In the first case, the compressive force is large enough to balance the tensile force, and an equilibrium will be reached, with a continuous liquid film completely contained within the nominal contact region. In the second case, the tensile force dominates the compressive force, and the interface will collapse into a nearly full contact.

2.2 Compressive Stresses

When the average gap between the two surfaces reduces, the asperities on the two surfaces further interact with each other and increased solid-solid contact occurs. The elastic contact between the two rough surfaces is investigated using the multi-scale contact model developed by Jackson and Streator [21]. This model is based on representing the rough surface in multiple scale of roughness using a Fourier series. Thus, the surface profile is divided into different scales of frequency, and the deformation of each spectral component is calculated separately using an appropriate model for the contact of a single asperity. In this work, a sinusoidal geometry is considered for the single asperity model. The analytical solutions of Johnson, Greenwood, and Higginson [JGH] [1] for early contact and near complete contact, and the empirical equation developed by Jackson and Streator [21] for contact area along with the surface separation relations developed by Rostami and Jackson [24] are used in the framework of the JS model to solve the contact problem.

2.2.1 Elastic contact of sinusoidal asperities

A contour plot of the sinusoidal geometry considered in this work is shown in Fig. 3. JGH [1] presented two asymptotic solutions analytically for the early and near complete contact of asperities. Jackson and Streator [21] presented an empirical equation connecting the two asymptotic solutions based on the numerical data provided by JGH [1].

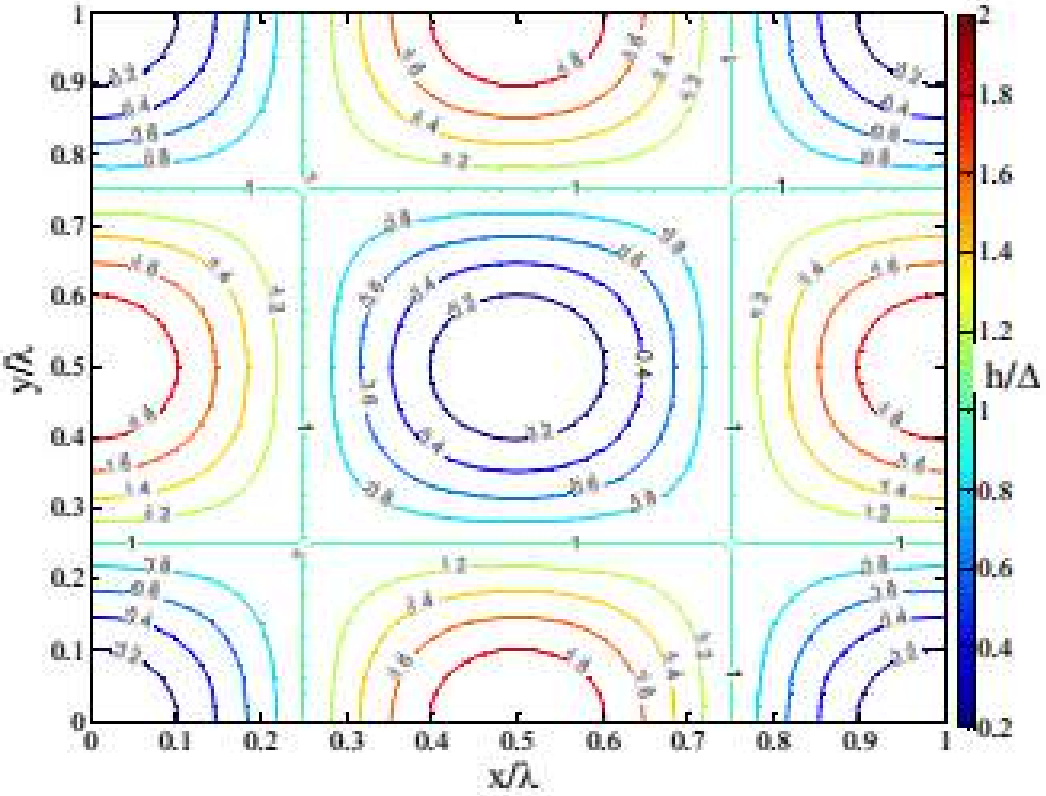

Figure 3. Contour plot of the 3D sinusoidal geometry.

JGH [1] solutions for contact area only consider elastic deformation during contact of three-dimensional sinusoidal shaped surfaces. In their work, $\overline{p}$ is defined as the average pressure (considering both contacting and non-contacting regions) acting on the surfaces, and p^* is defined as the average pressure that when applied to the asperity causes complete contact. p^* is given as

$$p^* = \sqrt{2}\pi E' \Delta f \qquad (7)$$

where Δ is the amplitude of the sinusoidal asperity, f is the spatial frequency or reciprocal of the asperity wavelength, λ $\left(f = 1/\lambda\right)$, and E' is the equivalent elastic modulus which is given by

$$\frac{1}{E'}=\frac{1-\nu_1^2}{E_1}+\frac{1-\nu_2^2}{E_2} \quad (8)$$

E_1,ν_1 and E_2,ν_2 are the elastic moduli and Poisson's ratios of the contacting surfaces.

The contacting flat surface is rigid, so, Eq. (8) reduces to

$$E'=\frac{E_1}{1-\nu^2} \quad (9)$$

The JGH [1] solutions are applicable when $\bar{p} \ll p^*$ i.e. at the early stages of contact, and when $\bar{p}$ approaches p^* ($\bar{p} \to p^*$) i.e. near the complete contact. The equations are given as shown

$$\bar{p} \ll p^*: \quad (A_{JGH})_1=\frac{\pi}{f^2}\left[\frac{3}{8\pi}\frac{\bar{p}}{p^*}\right]^{2/3} \quad (10)$$

$$\bar{p} \to p^*: (A_{JGH})_2=\frac{1}{f^2}\left(1-\frac{3}{2\pi}\left[1-\frac{\bar{p}}{p^*}\right]\right) \quad (11)$$

Empirical equations developed by Jackson and Streator [21] based on data provided by JGH [1], linking Eqs. (10) and (11) are given by

$$\text{for } \frac{\bar{p}}{p^*}<0.8: A=(A_{JGH})_1\left(1-\left[\frac{\bar{p}}{p^*}\right]^{1.91}\right)+(A_{JGH})_2\left(\frac{\bar{p}}{p^*}\right)^{1.84} \quad (12)$$

$$\text{for } \frac{\bar{p}}{p^*}\geq 0.8: A=(A_{JGH})_2 \quad (13)$$

Also, the asymptotic solutions for the surface separation for the early and near complete contact conditions of sinusoidal asperities developed by JGH [1] are presented as

$$\text{for } \frac{\bar{p}}{p^*}\ll 1: \left(\frac{\bar{g}}{\Delta}\right)_1=1-\frac{1}{2}\left(3\pi^2\frac{\bar{p}}{p^*}\right)^{2/3}+4\ln\left(\sqrt{2}+1\right)\left(\frac{\bar{p}}{p^*}\right) \quad (14)$$

$$\text{for } \frac{\bar{p}}{p^*}\to 1: \left(\frac{\bar{g}}{\Delta}\right)_2=\frac{16}{15\pi^2}\left(\frac{3}{2}\right)^{3/2}\left[1-\frac{\bar{p}}{p^*}\right]^{3/2} \quad (15)$$

Rostami and Jackson [24] developed an empirical equation for the average surface separation between sinusoidal asperities for the whole range of elastic contact connecting Eqs. (14) and (15) which is given by

$$\frac{\bar{g}}{\Delta}=\left(1-\left(\frac{\bar{p}}{p^*}\right)^{1/2}\right)^{3/2} \tag{16}$$

A two-dimensional schematic representation of the surface separation in sinusoidal asperity contacts before and during contact stages is shown in Fig 4. The average surface separation, $\bar{g}$, is equal to the amplitude of the sinusoidal asperity, Δ, when the two surfaces touch each other, while during the contact, the average surface separation, $\bar{g}$, is smaller than the amplitude of the sinusoidal asperity, Δ. In other words, when the average pressure between the two surfaces, $\bar{p}$, is equal to the complete contact pressure, p^*, the sinusoidal surface is completely flatten out and there is no gap between the surfaces, whereby $\bar{g}=0$.

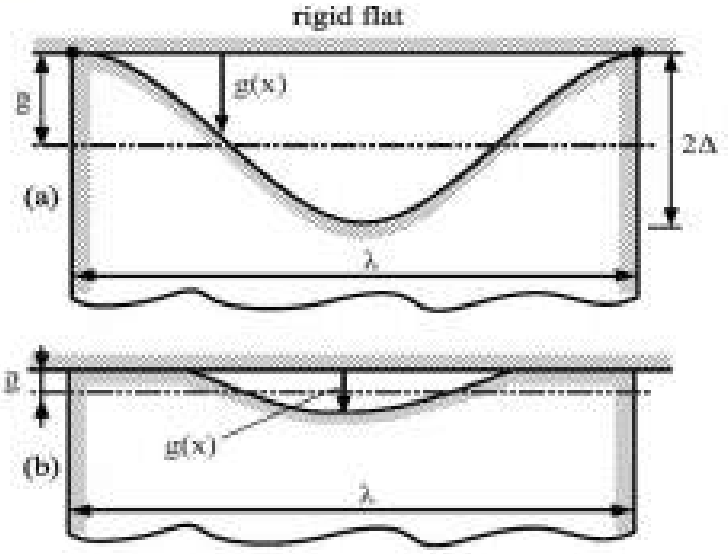

Figure 4. A 2D representation of contact between a sinusoidal asperity and a rigid flat (a) before, and (b) during contact.

Eqs. (12), (13), and (16) are embedded in the (JS) multi-scale contact model to solve the solid-solid contact of rough surfaces in the current work.

2.2.2 JS multi-scale contact model

Jackson and Streator [21] developed a multi-scale model for the contact between rough surfaces based on a spectral approach, and is briefly summarized. The model is based on the following assumptions [21]:

1. Asperities of smaller cross-sectional surface area are located on top of larger asperities.
2. Each scale or level of frequency carries the same total load.
3. At each frequency level, the load is shared equally among the contacting asperities.
4. At each frequency level, each asperity deforms according to a chosen asperity contact model (elastic sinusoidal asperity contact in the current work).
5. The asperities of a certain level of frequency cannot be deformed more than the amplitude or height of the asperities at that level.

The average pressure, $\overline{p}_k$, at frequency level, k, can be obtained based on the assumptions #2 and #3

$$\overline{p}_k = \frac{F}{A_{k-1}} \tag{17}$$

where F is the total force between the contacting rough surfaces, and A_{k-1} is the contact area at the frequency level $k-1$ which acts as the nominal contact area for the frequency level k. Using the single asperity relations, the contact area and average surface separation of a single asperity at frequency level k under the contact pressure $\overline{p}_k$ can be calculated from Eqs. (12), (13), and (16) i.e. $\overline{A}_k = f(\overline{p}_k)$ and $\overline{g}_k = f(\overline{p}_k)$. Then, the contact area at the frequency level k can be calculated

$$A_k = N_k \overline{A}_k \tag{18}$$

In Eq. (18), N_k is the number of asperities in contact at frequency level k, and can be calculated by

$$N_k = \eta_k A_{k-1} \tag{19}$$

where η_k is the number of asperities per unit area and is related to the k level frequency $f_k = 1/\lambda_k$ by

$$\eta_k = 2 f_k^2 \tag{20}$$

The 3D rough surface considered in this work is comprised of oscillations both in x and y directions (Fig. 1). In JS multi-scale model, a single amplitude for each frequency scale is required based on a 1D discrete Fourier transform (DFT), of a 2D surface profile (i.e. $z(x)$), while for a 3D surface profile (i.e. $z(x,y)$) a matrix of coefficients is obtained by calculating the 2D DFT. Therefore, to apply the JS model to a 3D topography, an

equivalent amplitude is calculated from the matrix of Fourier coefficients arising from the 2D DFT. Now, the 2D DFT can be expressed as

$$F(k_x,k_y)=\frac{1}{N_xN_y}\sum_{n_x=0}^{N_x-1}\sum_{n_y=0}^{N_y-1}z(n_x,n_y)e^{-i2\pi(k_xn_x/L_x+k_yn_y/L_y)} \quad (21)$$

where k_x and k_y correspond to the spatial frequencies in x and y directions, while n_x and n_y correspond to the spatial coordinates in x and y directions. The output is a $N_x \times N_y$ matrix comprising of complex elements. As the current model requires a single amplitude for each frequency scale, an equivalent 1D Fourier coefficient is calculated based on (25)

$$\beta_k=\frac{1}{2}\left[\sqrt{\sum_{k_y=0}^{N_y-1}|F(k,k_y)|^2}+\sqrt{\sum_{k_x=0}^{N_x-1}|F(k_x,k)|^2}\right] \quad (22)$$

The above equation is based on calculating the r.m.s. values of 1D Fourier coefficients in x and y directions and then averaging the two values. It can be shown that Δ_k is related to the equivalent 1D amplitude coefficient, β_k, via the simple relation, $\Delta_k=2\beta_k$, except at $k=N/2$, where $\Delta_{N/2}=\beta_{N/2}$.

2.3 Contact Model Including both Tensile and Compressive Stresses

In order to consider the effect of liquid film in contact between rough surfaces, the average gap between two surfaces and also the area over which the liquid film acts are needed to be determined. A volume-loss approach due to both compressive and tensile stresses is used to consider the effect of liquid film. This approach is based on calculating the reduction in the average gap between the two surfaces in the wetted region based on the compressive and tensile volume losses. In the next sections, it is explained how to calculate the volume losses due to compressive and tensile stresses.

2.3.1 Volume loss due to compressive stresses

The loss in available volume due to compressive stresses can be calculated by summing up the volume losses at different frequency scales based on the JS multi-scale model. Each frequency scale experiences a separate volume reduction. In order to calculate the volume loss in each frequency scale, the reduction in the average gap in each frequency scale is calculated. The initial average gap at each frequency scale is equal to the amplitude at that frequency scale when there is no force acting on the

contacting surfaces. In the presence of force the average gap reduction at frequency scale k can be calculated as

$$(\Delta\bar{g}_k)_c = \Delta_k - \bar{g}_k = \Delta_k\left(1-\left(1-\left(\frac{\bar{p}_k}{p_k^*}\right)^{1/2}\right)^{3/2}\right) \quad (23)$$

where $(\Delta\bar{g}_k)_c$ is the reduction in average gap at frequency scale k due to compressive stresses. This reduction multiplied by the contact area at frequency level $k-1$ (which acts as a nominal contact area for frequency scale k) gives the volume loss associated with the frequency scale k. Therefore, the total volume loss due to compressive stresses, ΔV_c, can be calculated by

$$\Delta V_c = \sum_{k=1}^{k_{max}} (\Delta\bar{g}_k)_{comp} A_{k-1} \quad (24)$$

2.3.2 Volume loss due to tensile stresses

The liquid film also tends to reduce the average gap between surfaces by inducing tensile stresses between surfaces due to capillary pressure. In the presence of a liquid film, the solutions for the solid-solid contact are not strictly valid anymore. However, the solutions are still used in the current work to calculate contributions of the compressive stresses in the contact between surfaces. In calculation of the volume loss due to tensile stresses, it is assumed that the real contact area is a small fraction of the nominal contact area (an assumption that is to be validated later). Thus, ignoring the regions of solid-solid contact, it follows that the tension throughout the wetted region is uniform and equal in magnitude to the Laplace-Young pressure. This assumption of pressure uniformity is invalid after the point of surface collapse because then the ratio of real contact area to nominal contact area is no longer expected to be small. Therefore, the methods used here to solve the contact problem are valid up to the point where instability occurs (i.e., to the point of surface collapse). For a uniform pressure, Δp, acting on a circular wetted area with radius, r_w, the deformation in the wetted region can be obtained by (26)

$$u_z(r) = \frac{4}{\pi E^*}\Delta p r_w E(r/r_w) \qquad r \le r_w \quad (25)$$

where $u_z(r)$ denotes the elastic deformation at radial position r measured from the center of rectangular domain (Fig. 1), and $E(r/r_w)$ is the complete elliptic integral of the second

kind. Integrating Eq. (25) over the wetted region, the volume loss due to tensile stresses, ΔV_t, can be calculated by

$$\Delta V_t = \int_0^{r_w} u_t(r)(2\pi r dr) \quad (26)$$

Substituting and rearranging Eq. (25) in Eq. (26), the following relation can be obtained

$$\Delta V_t = \frac{8\Delta p r_w}{E'} \int_0^{r_w} rE\left(r / r_w\right) dr \quad (27)$$

Integrating Eq. (27), the following relation for volume loss due to tensile stresses can be obtained

$$\Delta V_t = \frac{16}{3} \frac{\Delta p}{E'} r_w^3 \quad (28)$$

Substituting for the pressure drop from Eq. (6) in Eq. (28), the following relation for the volume loss due to tensile stresses can be obtained

$$\Delta V_t = \frac{16}{3} \frac{\gamma\left(\cos\theta_A + \cos\theta_B\right)}{\bar{h}E'} r_w^3 \quad (29)$$

where the volume loss due to tensile stresses for a certain liquid is only a function of average gap, $\bar{h}$, and the wetted radius, r_w. Also, the tensile force, F_t, can be related to the Laplace-Young pressure according to the following relation

$$F_t = \pi r_w^2 \Delta p \quad (30)$$

where F_t is the tensile force between the rough surfaces. Substituting for the Laplace-Young pressure from Eq. (6), the relation below can be obtained

$$F_t = \frac{\pi \gamma r_w^2}{\bar{h}} \left(\cos\theta_A + \cos\theta_B\right) \quad (31)$$

The total volume loss in the wetted region, ΔV_{tot}, is calculated by summing the volume loss due to compressive stresses in the wetted region, and the volume loss due to tensile stresses, ΔV_t.

$$\Delta V_{tot} = \left(\frac{\pi r_w^2}{A_n}\right) \Delta V_c + \Delta V_t \quad (32)$$

The coefficient multiplying ΔV_c (which is the compressive volume loss over the entire nominal contact region) is needed to account for the fact that we are interested in the total volume loss within the wetted region.

When the two surfaces come into contact at zero load, the gap between the two surfaces is the maximum height of the rough surface, z_{max}. During loading, the deformation due to both compressive and tensile stresses causes a change in the average gap between the surfaces. The new average gap within the wetted region can be obtained using the total volume loss

$$\bar{h} = z_{max} - \frac{\Delta V_{tot}}{\pi r_w^2} = z_{max} - \frac{\Delta V_c}{A_n} - \frac{\Delta V_t}{\pi r_w^2} \tag{33}$$

Enforcing the volume conservation of the liquid film, the following relation between the average gap and the radius of the wetted region can be obtained

$$V_0 = \pi r_w^2 \bar{h} \tag{34}$$

This relationship can be written alternatively by

$$r_w = \left(V_0 / \pi \bar{h}\right)^{1/2} \tag{35}$$

Substituting for the average gap between the surfaces from Eq. (33)

$$r_w = \left(\frac{V_0}{\pi \left(z_{max} - \frac{\Delta V_c}{A_n} - \frac{\Delta V_t}{\pi r_w^2} \right)} \right)^{1/2} \tag{36}$$

Due to the nonlinear dependency of the both compressive and tensile stresses on the radius of the wetted region, Eq. (36) must be solved iteratively. It should be noted that the compressive volume loss depends on the total force between the two surfaces, which is the sum of the external load, P, and the tensile force, F_t. The compressive force, F_c, is given by

$$F_c = P + F_t \tag{37}$$

where F_t can be calculated from Eq. (31).

2.3.3 Numerical solution algorithm

The numerical algorithm used to solve the rough surface contact problem in the presence of liquid film is shown in Fig 5. The material and geometrical parameters of the contacting rough surfaces and the liquid volume are needed in the numerical algorithm. When the two surfaces touch each other, the initial average gap is equal to the maximum height of the rough surface. As the surfaces come into contact, the average gap will change, and the new average gap and radius of wetted region are obtained using Eqs. (33) and (36). The iteration process will continue until convergence is acquired. Convergence or divergence of the iteration process is determined based on the relative error of the tensile force in two successive iterations ($\left|F_{i-new}-F_{i-old}\right|/F_{i-old}$. Convergence is accomplished when the relative error is less than 10^{-3} .

3. Results

The results of the numerical model developed for the contact between rough surfaces in the presence of liquid film are presented in this section. The input parameters such as rough surface nominal contact area, A_a, surface topography, $z(x,y)$, effective elastic modulus, E', liquid volume, V_0, liquid surface tension, γ, and contact angles ,$\theta_{A,B}$, are needed to obtain a set of results. For convenience, a zero value is selected for contact angles of the liquid film with upper and lower surfaces, $\theta_{A,B}=0$. Three-dimensional Gaussian isotropic surfaces generated by computer are used for the simulations. It was shown [27] that the statistical features of many random profiles such as distribution of heights, curvatures, slopes, and peak density could be expressed in terms of two parameters, namely the r.m.s.roughness, σ, and the correlation length, l_c. In this work, a surface generation method outlined by Garcia and Stoll [28] is implemented, where an uncorrelated distribution of surface points using a random number generator is convolved with a Gaussian filter to achieve a random Gaussian rough surface with a prescribed standard deviation and having an exponential autocorrelation function with a prescribed correlation length.

The numerical algorithm shown in Fig.5 is used to obtain the equilibrium configuration for a given surface topography with the reference material and geometrical properties given in Table 1. The simulated rough surface has a Gaussian isotropic distribution with correlation length to side length ratio of $l_c/L=1/200$. The results for the tensile force, F_z , average gap, $\bar{h}$, wetted radius, r_w, and real contact area, A_r, versus the flexibility of the rough surface, $1/E'$, in the absence of external load, $P=0$, are shown in Fig.6.

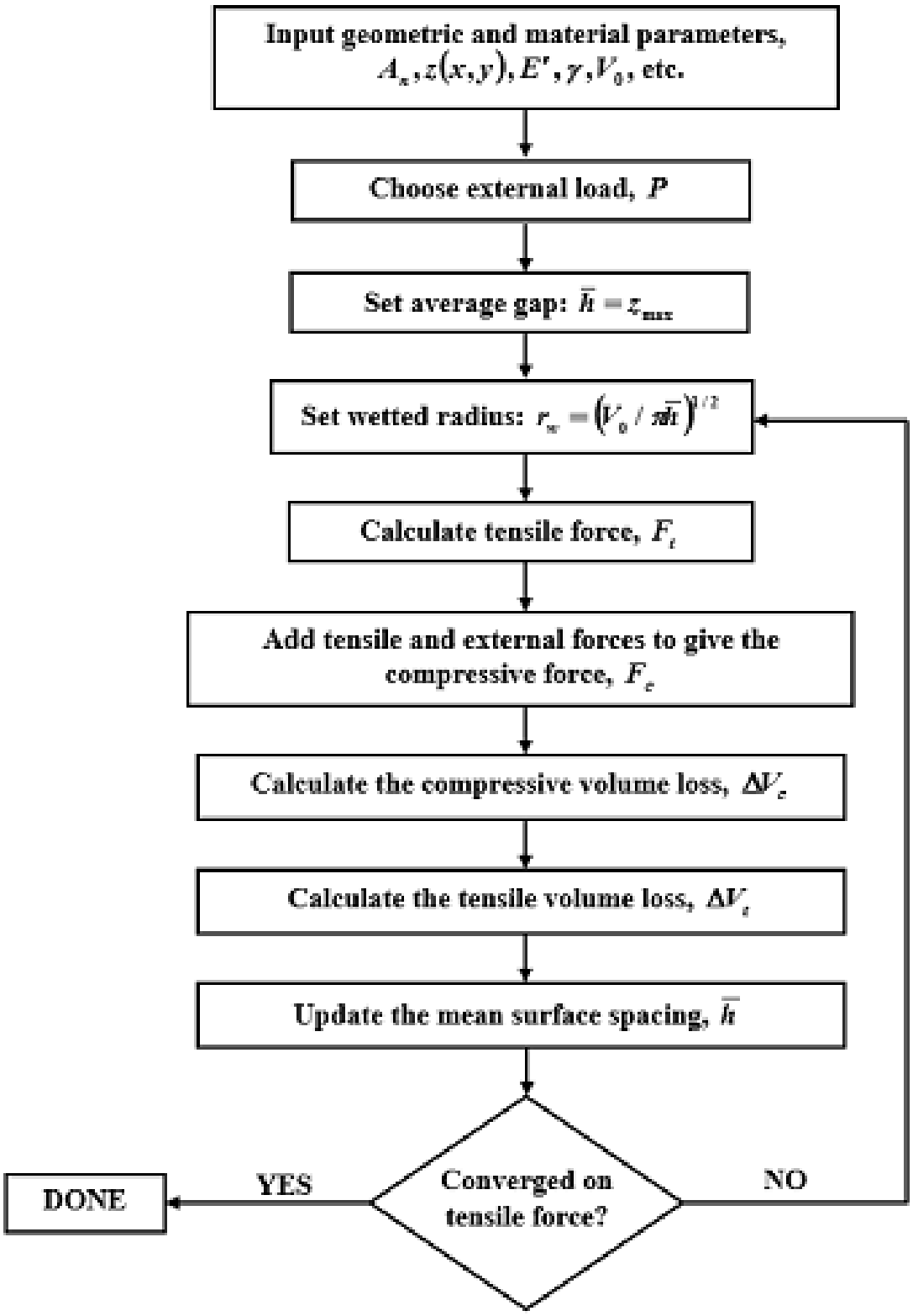

Figure 5. Flowchart of the numerical algorithm

Table 1 Reference properties

$V_0 = 0.1\ mm^3$	$\sigma = 0.4\ \mu m$
$\gamma = 72.7\ mN/m$,	$A_a = 4\ cm^2$

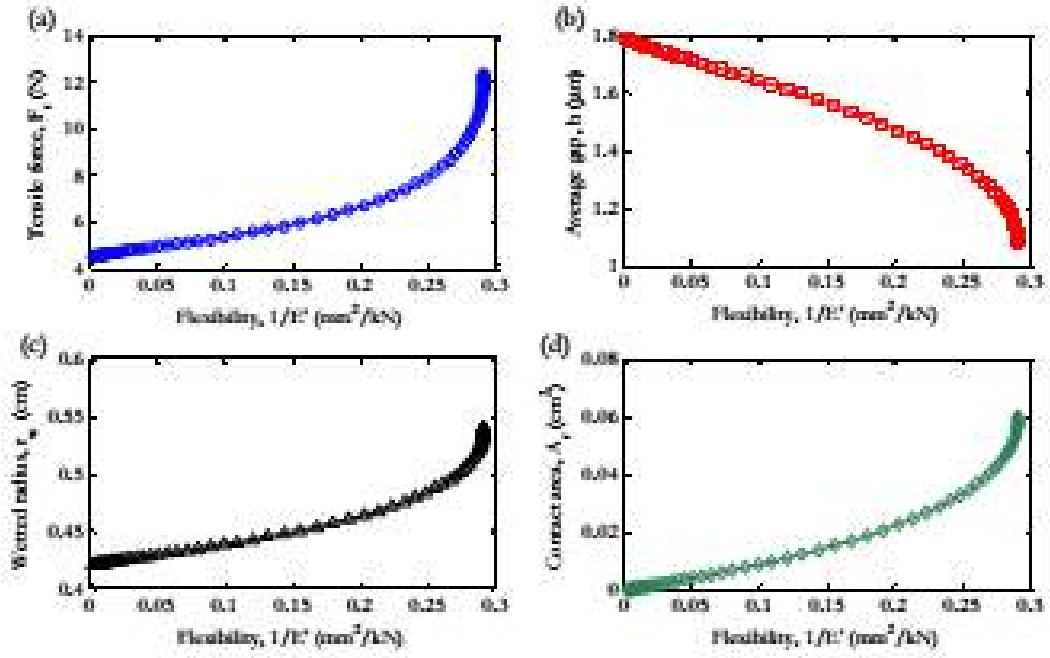

Figure 6. The results for (a) tensile force, (b) average gap, (c) wetted radius, and (d) contact area versus the flexibility of the rough surface.

In Fig. 6, tensile force, F_t, contact area, A_r, and the radius of wetted region, r_w, increase, while the average gap decreases with the flexibility of the rough surface until the slope of the curve becomes vertical. The last data point on the curve (to a resolution of $10^{-6}\ mm^3/kN$ in the value of flexibility) is taken as the point of instability, and it means that no equilibrium configuration could be obtained for the contact problem for higher values of flexibility. For higher flexibilities, then, the tensile force overwhelms the compressive force and the two surfaces are predicted to experience near-complete or complete contact (i.e. surface collapse).

The results for the tensile force, average gap, wetted radius, and contact area versus the external load applied between the contacting rough surfaces for the material and geometrical properties given in Table 1 are shown in Fig. 7. It should be noted the results in Fig. 7 are obtained based on the flexibility value of $1/E' = 0.02\ \text{mm}^2/\text{kN}$.

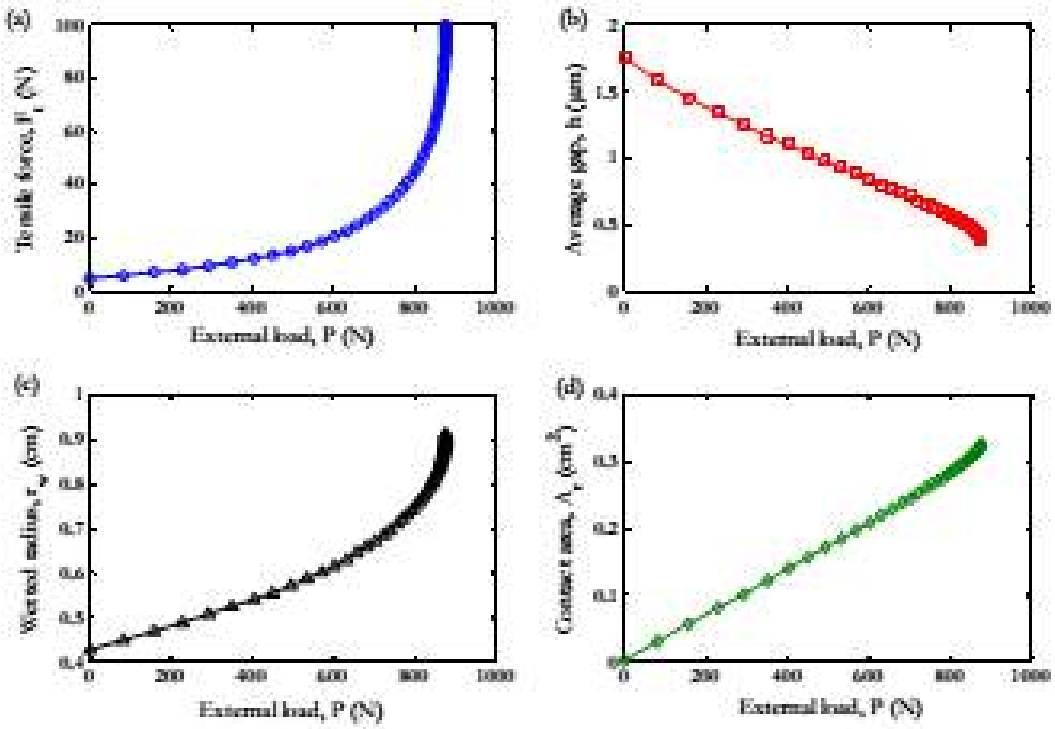

Figure 7. The results for (a) tensile force, (b) average gap, (c) wetted radius, and (d) contact area versus the external load between contacting surfaces.

As it can be seen in Fig. 7, the tensile force, wetted radius, and contact area increase while the average gap decreases with the external load. As external load, P, increases, it causes more interaction between the contacting surfaces, which causes a reduction in average gap, $\bar{h}$, between the surfaces and also an increase in the contact area, A_r, between the surfaces. As the gap between the surfaces decreases, the liquid volume between the surfaces spreads over a wider area, which means that the radius of wetted

region, r_n, increases. The reduction in average gap and the increase in the wetted area causes the tensile force, F_t, to increase.

3.1 Non-dimensionalization:

In this section, we seek normalization to present the results in the most general way. By substituting for the radius of wetted region, r_n, from Eq.(35) in Eq.(31), we have

$$F_t = \frac{\gamma V_0}{\bar{h}^2}\left(\cos\theta_A + \cos\theta_B\right) \tag{38}$$

Considering the case with no external load, $P=0$, the compressive force on a given surface balances the tensile force ($F_c = F_t$). Also, ignoring the effect of tensile stresses on the average gap in initial contact, the average gap for the first frequency scale $(k=1)$ can be related to the load by Eq.(16)

$$\frac{\bar{g}_1}{\Delta_1} = \left(1 - \left(\frac{F_t}{A_n \bar{p}_1}\right)^{1/2}\right)^{3/2} \tag{39}$$

where the average pressure in the first frequency, $\bar{p}_1$, is calculated by dividing the tensile force, F_t , by the nominal contact area at the first frequency level, A_n. The complete contact pressure at the first frequency can be calculated using Eq.(7) with Eq.(39)

$$\frac{\bar{g}_1}{\Delta_1} = \left(1 - \left(\frac{F_t}{\sqrt{2\pi}E^* A_n^{1/2}\Delta_1}\right)^{1/2}\right)^{3/2} \tag{40}$$

Now substituting Eq.(38) in (40)

$$\bar{g}_1 = \Delta_1\left(1 - \left(\frac{\gamma V_0\left(\cos\theta_A + \cos\theta_B\right)}{\sqrt{2\pi}A_n^{1/2}E^*\Delta_1\bar{h}^2}\right)^{1/2}\right)^{3/2} \tag{41}$$

Supposing that the average gap at frequency level 1, $\bar{g}_1$, is related to the overall gap, $\bar{h}$, by some factor X such that $\bar{g}_1 = X\bar{h}$. Then we can conclude

$$\frac{\bar{h}}{\sigma} = \frac{1}{X}\frac{\Delta_1}{\sigma}\left(1 - \left(\frac{\gamma V_0\left(\cos\theta_A + \cos\theta_B\right)}{\sqrt{2\pi}A_n^{1/2}E^*\sigma^2\left(\Delta_1/\sigma\right)\left(\bar{h}/\sigma\right)^2}\right)^{1/2}\right)^{3/2} \tag{42}$$

where the r.m.s. roughness, σ, is used as a scaling factor. It can be deduced from Eq. (42)

$$\frac{\bar{h}}{\sigma} = \bar{f}\left(\frac{\gamma W_0 (\cos\theta_A + \cos\theta_B)}{\sqrt{2}\pi A_a^{1/2} E' \sigma^3}, \frac{\Delta_1}{\sigma}, X \right) \tag{43}$$

where $\bar{f}$ is an unknown function, Δ_1 and σ are specified by the undeformed surface profile, so, Δ_1 / σ is a geometric parameter. In contrast, X relates the parameters that result from deformation, i.e. $\bar{g}_1$ and $\bar{h}$. However, it can be shown that, for a given σ, X depends only on the details of the surface profile (i.e. the set of amplitude coefficients). Therefore, Eq. (43) implies that the equilibrium gap for a given surface profile depends only on the dimensionless parameter $\gamma W_0 (\cos\theta_A + \cos\theta_B) / \sqrt{2}\pi A_a^{1/2} E' \sigma^3$. Therefore, an adhesion parameter is defined as

$$\Gamma = \frac{\gamma W_0 (\cos\theta_A + \cos\theta_B)}{\sqrt{2}\pi A_a^{1/2} E' \sigma^3} \tag{44}$$

Considering the external load introduces another parameter into the dependence of $\bar{h} / \sigma$ on the input parameters. Also, consideration of the direct effect of tensile stresses introduces the additional dimensionless ratio $V_0 / A_a \sigma$ which we label as V_0^* and refer to as the dimensionless volume. The dimensionless tensile force, F_t^* and external force, P^*, can be expressed as

$$F_t^* = \frac{F_t}{\gamma W_0 (\cos\theta_A + \cos\theta_B) / \sigma^2} = \left(\frac{\sigma}{\bar{h}} \right)^2 \tag{45}$$

$$P^* = \frac{P}{\gamma W_0 (\cos\theta_A + \cos\theta_B) / \sigma^2} \tag{46}$$

In general, for a given rough surface profile, we can write

$$\frac{\bar{h}}{\sigma} = \bar{f}^* (\Gamma, P^*, V_0^*) \tag{47}$$

where $\bar{f}^*$ is an unknown function. Alternatively, using Eq. (45), we obtain

$$F_t^* = \bar{f}^{**} (\Gamma, P^*, V_0^*) \tag{48}$$

where $\bar{f}^{**}$ denotes another unknown function. For a given surface topography, Eqs. (47) and (48) are the most general expressions for the equilibrium average gap and tensile force, respectively.

3.2 Equilibrium Curves

In this section, the results for non-dimensional tensile force, F_t^*, versus the non-dimensional adhesion parameter, Γ, for different material and geometrical parameters are presented. A convergence test is performed to obtain the number of numerical nodes needed along both x and y axes to get accurate results for a 3D Gaussian isotropic surface. As shown in Fig. 8, for each case the tensile force increases with increasing adhesion parameter until the curve becomes vertical. It can be seen that convergence is acquired for node numbers higher than 2000 along coordinate axis for a Gaussian isotropic surface with $l_c / L = 1/200$. Performing an extensive number of simulations for different Gaussian isotropic surfaces varying correlation length, l_c, and side length, L, it is shown that the convergence is guaranteed for simulated surfaces with at least 10 nodal points per correlation length. In the current work, the numerical results are obtained for the nominal contact area with $L = 2$ cm.

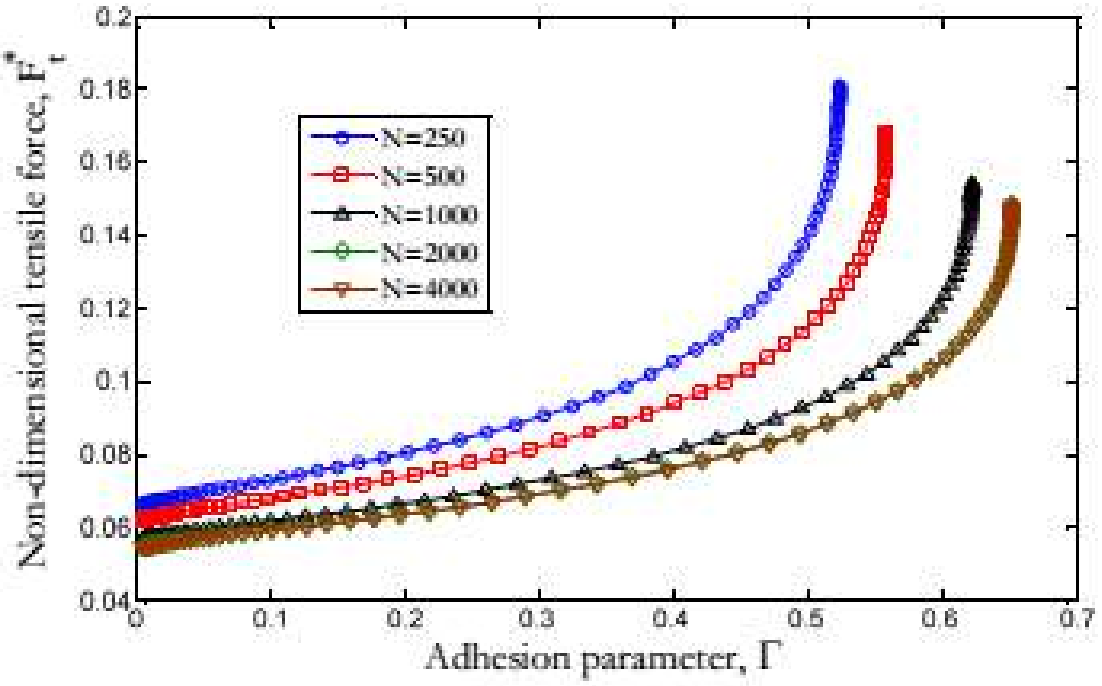

Figure 8. Non-dimensional tensile force results versus adhesion parameter for different number of nodes, N, along each coordinate axis.

As mentioned previously, the non-dimensional tensile force, F_t^*, is a function of adhesion parameter, Γ, non-dimensional external load, P^*, and non-dimensional liquid volume, V_0^*. The results for the dimensionless tensile force, F_t^*, versus the adhesion

parameter, Γ, for different values of dimensionless volume, V_0^*, in the absence of external load ($P^* = 0$) are shown in Fig 9. As expected, the normalized adhesion force increases with adhesion parameter for different values of the dimensionless volume until it reaches a vertical slope suggestive of surface collapse. As the non-dimensional liquid volume increases, the instability occurs at higher values of the adhesion parameter; however, the non-dimensional tensile force at the point of instability is nearly the same at each of the non-dimensional liquid volumes.

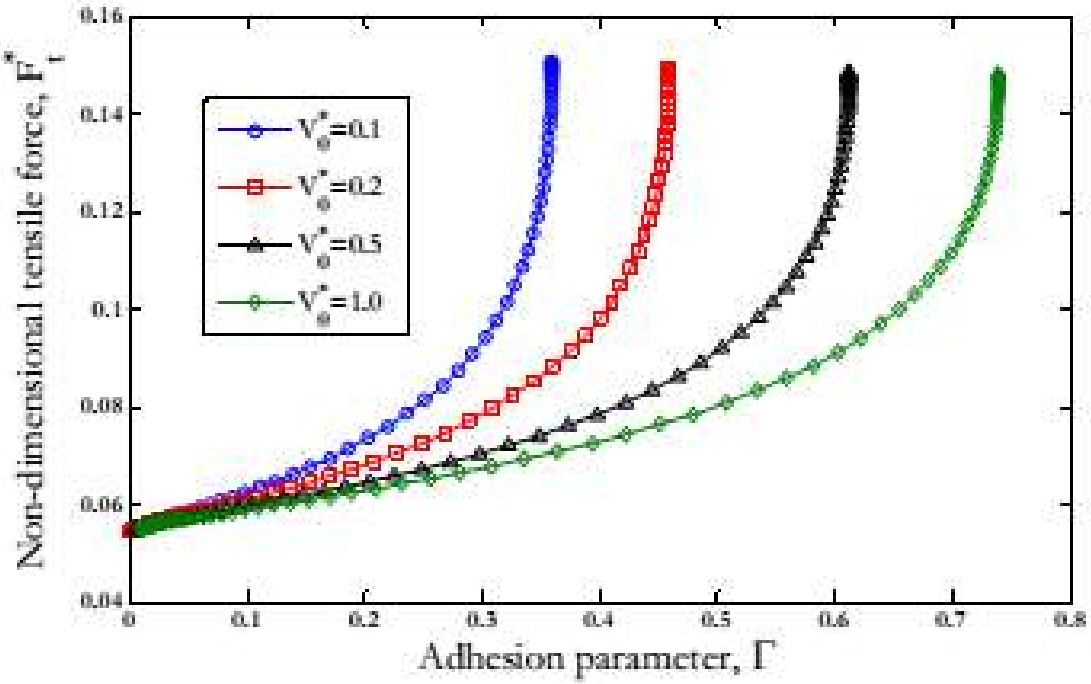

Figure 9. Non-dimensional tensile force versus adhesion parameter for different values of non-dimensional liquid volumes.

Fig. 10 shows the results for non-dimensional tensile force, F_t^*, versus the adhesion parameter, Γ, for different values of dimensionless external load, P^*. A constant value is selected for the non-dimensional liquid volume for all the cases in Fig. 10 ($V_0^* = 0.5$). It can be seen in Fig. 10, as the external load, P^*, increases the instability occurs at lower values of the adhesion parameter, Γ. Also, the non-dimensional tensile force, F_t^*, at the point of instability increases as the non-dimensional external load, P^*, increases.

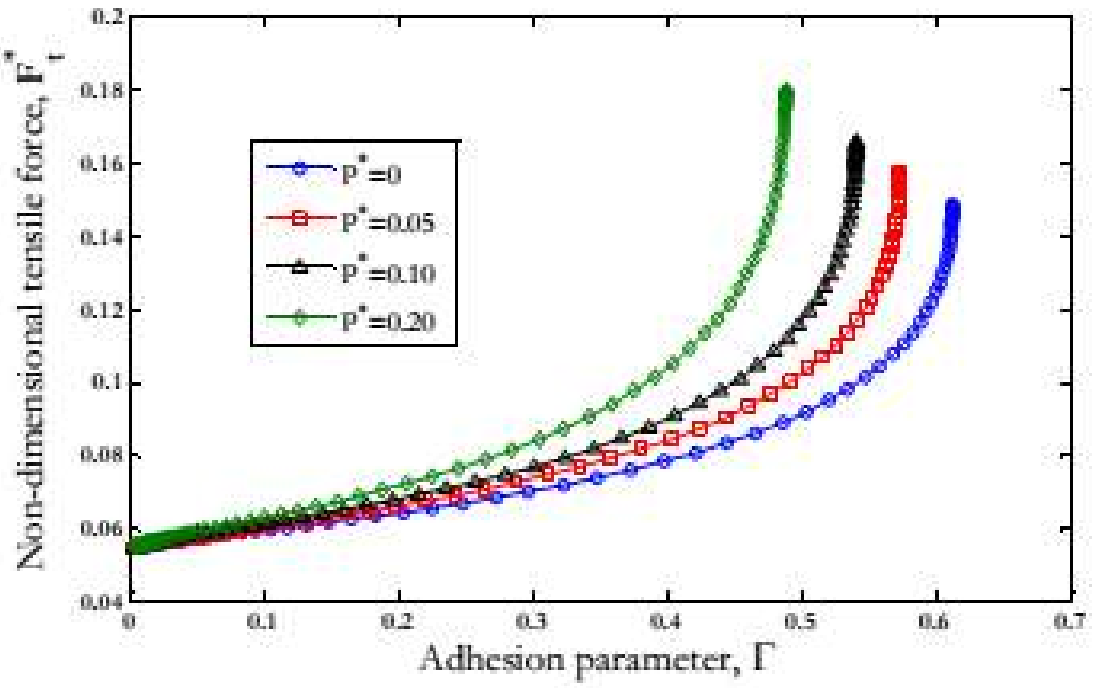

Figure 10. Non-dimensional tensile force versus adhesion parameter for different values of non-dimensional external load.

Results for the average gap normalized by the r.m.s. surface roughness, $h^* = \bar{h}/\sigma$, versus the adhesion parameter, Γ, are shown in Fig. 11 for different non-dimensional liquid volumes, V_0^*, where $P^* = 0$, and shown in Fig. 12 for non-dimensional external loads, P^*, where $V_0^* = 0.5$. As observed in Fig. 11, the non-dimensional average gap, h^*, decreases as the adhesion parameter, Γ, increases until the slope of the curve becomes vertical. Additionally, the instability occurs at higher values of adhesion parameter, Γ, as the non-dimensional liquid volume, V_0^*, increases. In Fig. 12, the instability happens at lower values of adhesion parameter, Γ, as the non-dimensional external load, P^*, increases. Also, Fig. 12 shows that as the non-dimensional external load, P^*, increases, the non-dimensional average gap, h^*, at the point of instability decreases.

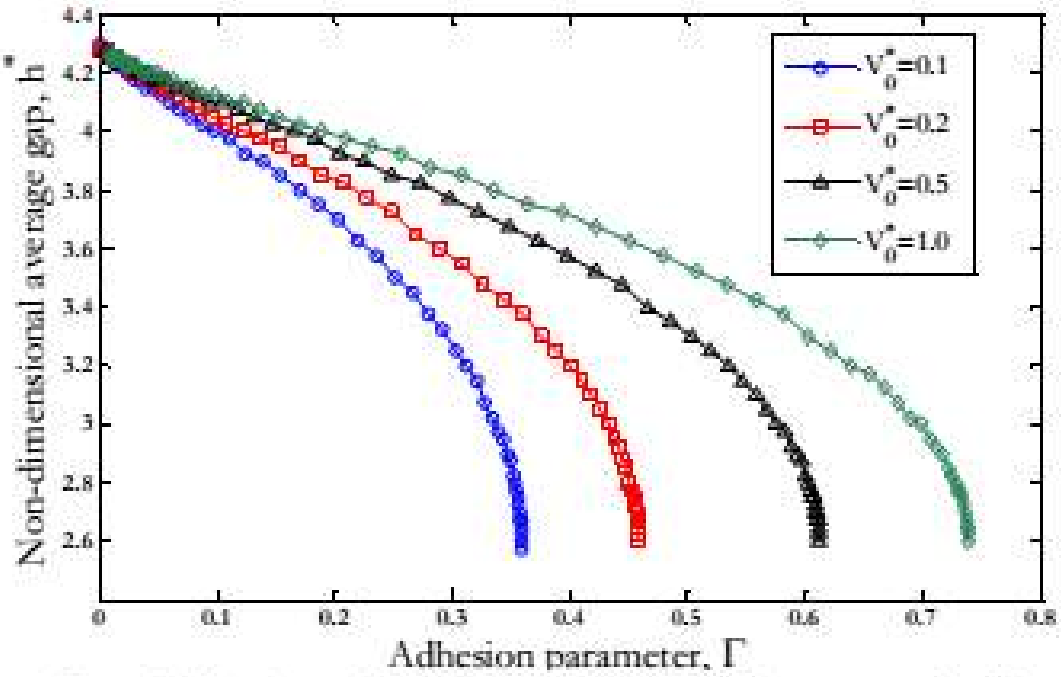

Figure 11. Non-dimensional average gap versus adhesion parameter for different values of non-dimensional liquid volume.

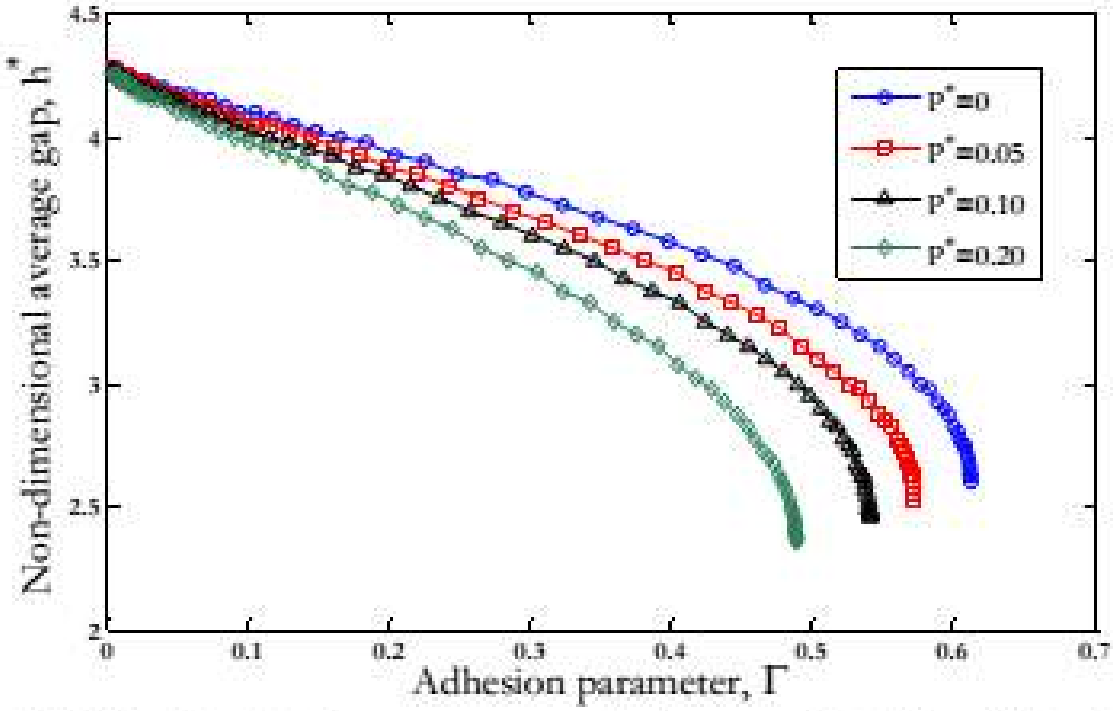

Fig.12 Non-dimensional average gap versus adhesion parameter for different values of non-dimensional external load.

The results for non-dimensional contact area, $A_r^* = A_r / A_a$, versus the adhesion parameter, Γ^*, are shown in Fig. 13 for different non-dimensional liquid volumes, V_0^*, where $P^* = 0$, and in Fig. 14 for non-dimensional external loads, P^*, where $V_0^* = 0.5$. As the non-dimensional liquid volume, V_0^*, increases, the non-dimensional contact area, A_r^*, at the point of instability also increases (Fig. 13). Likewise, as the non-dimensional external load, P^*, increases, the non-dimensional contact area, A_r^*, at the point of instability increases (Fig. 14). As it can be seen from Figs. 13 and 14, the non-dimensional contact area, A_r^*, is less than 2% at the point of instability, which validates the model assumption that the real contact area is a small fraction of nominal contact area.

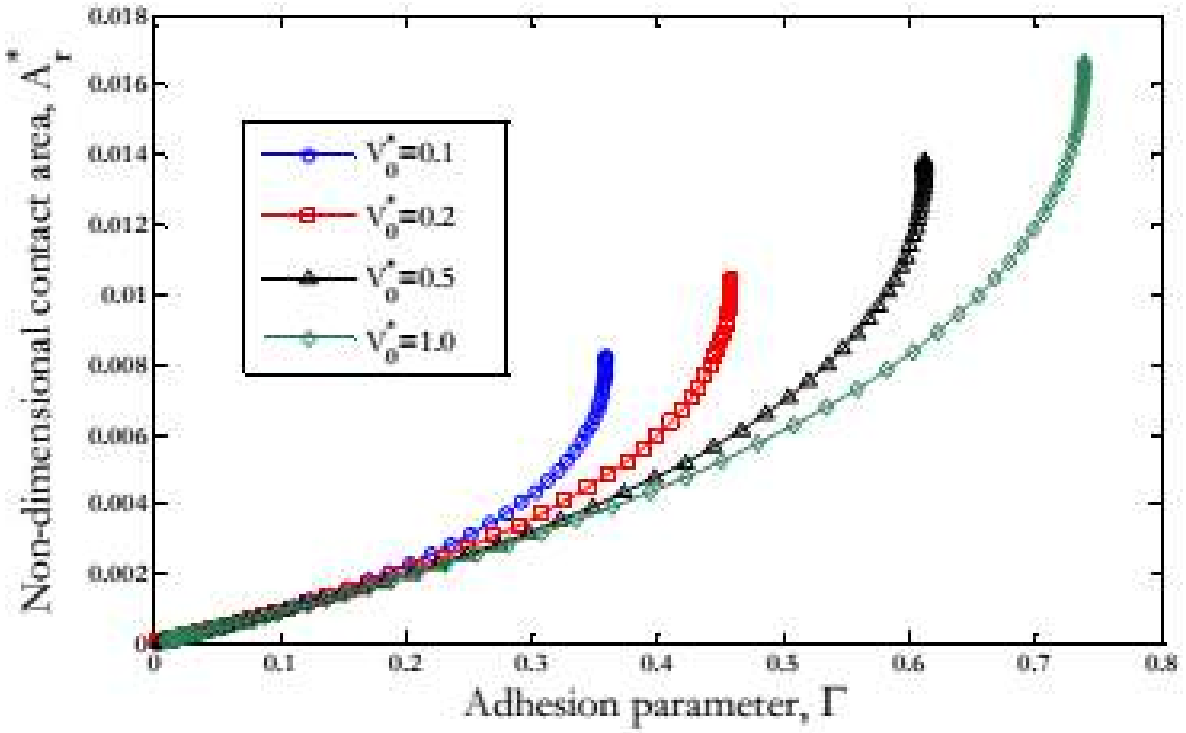

Figure 13. Non-dimensional contact area versus adhesion parameter for different values of non-dimensional liquid volume.

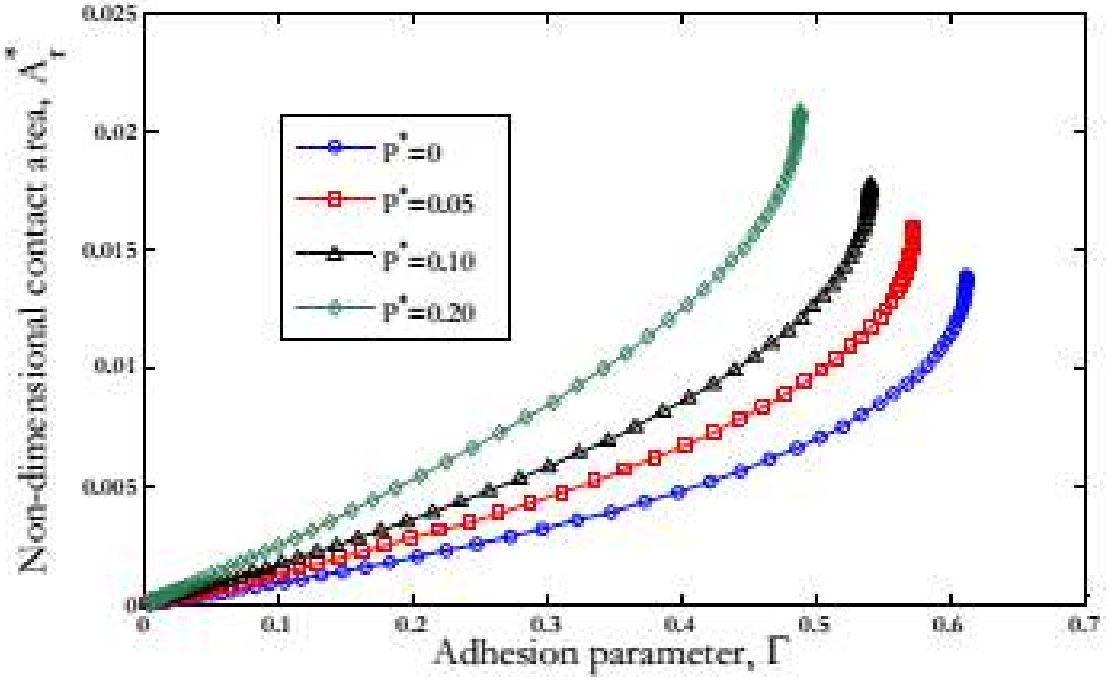

Figure 14. Non-dimensional contact area versus adhesion parameter for different values of non-dimensional external load.

3.3 Critical Adhesion Parameter

It is of interest to predict the point of instability in liquid-mediated contact between solid surfaces, as beyond this point, the surfaces would experience strong adhesion or stiction. In this section, the goal is to obtain a relation for the point of instability based on material and geometrical properties of the rough surfaces and the liquid film. Presenting a general relation that is applicable to all rough surfaces including both Gaussian and non-Gaussian random rough surfaces is not feasible. However, restricting our attention to rough surfaces with an isotropic Gaussian distribution simplifies the task. It can be concluded from Figs. (9-14) that the critical adhesion parameter, Γ_{cr}, for a given rough surface is a function of non-dimensional liquid volume, V_0^*, and non-dimensional external load, P^*, i.e. $\Gamma_{cr} = f\left(P^*, V_0^*\right)$. The results in Figs. (9-14) were obtained for a given rough surface with r.m.s. roughness of $\sigma = 0.4$ μm, and having an isotropic Gaussian distribution with correlation length to side ratio of $l_c / L = 1/200$. The dependency of the critical adhesion parameter, Γ_{cr}, on the correlation length, l_c, of a Gaussian isotropic rough surface with

a given r.m.s. roughness, σ, is investigated in Fig. 15. The results in Fig. 15 are obtained for the critical adhesion parameter, Γ_{cr}, versus the non-dimensional maximum height, $z^*_{max} = z_{max}/\sigma$, of a Gaussian isotropic rough surface with r.m.s. roughness of $\sigma = 0.4$ μm. It can be seen that the critical adhesion parameter, Γ_{cr}, increases as the maximum height of the surface, z^*_{max}, increases, and it is independent of correlation length, l_c.

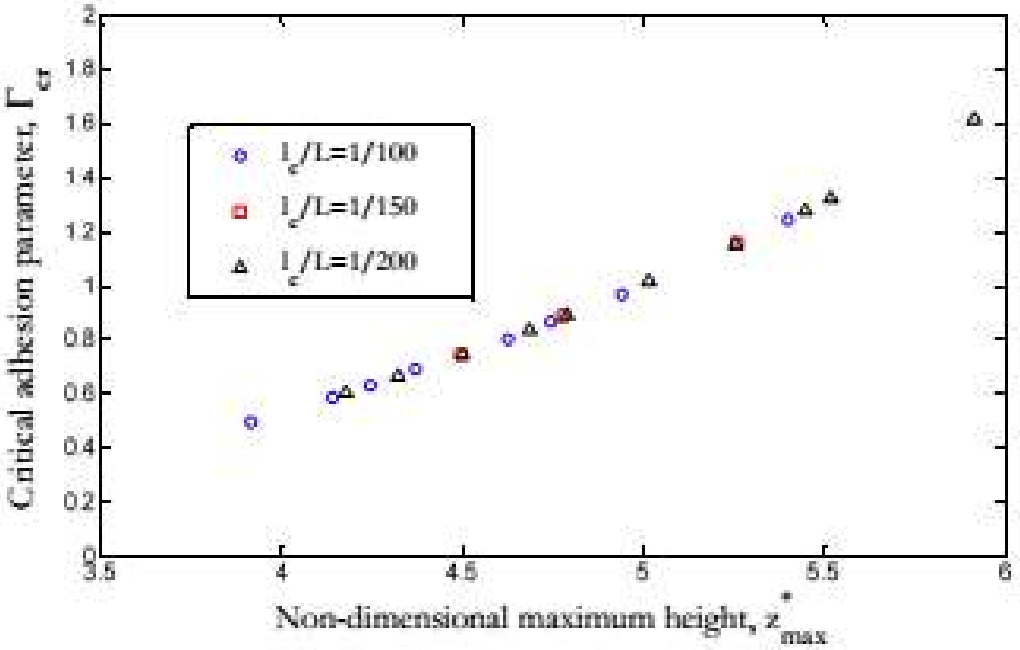

Figure 15. Critical adhesion parameter versus the non-dimensional maximum height for different values of correlation length.

In Fig. 16, the results are obtained for the critical adhesion parameter, Γ_{cr}, versus the non-dimensional maximum height, z^*_{max}, for different values of r.m.s. roughness, σ, while the correlation length is constant and set to $l_c/L = 1/200$. The results show that the critical adhesion parameter, Γ_{cr}, is also independent of r.m.s. roughness, which is a consequence of the normalization considered in this work. The results in Figs. 15 and 16 lead us to conclude that by considering the effect of maximum surface height, z^*_{max}, a general relation for critical adhesion parameter can be obtained, which is applicable to different Gaussian isotropic rough surfaces.

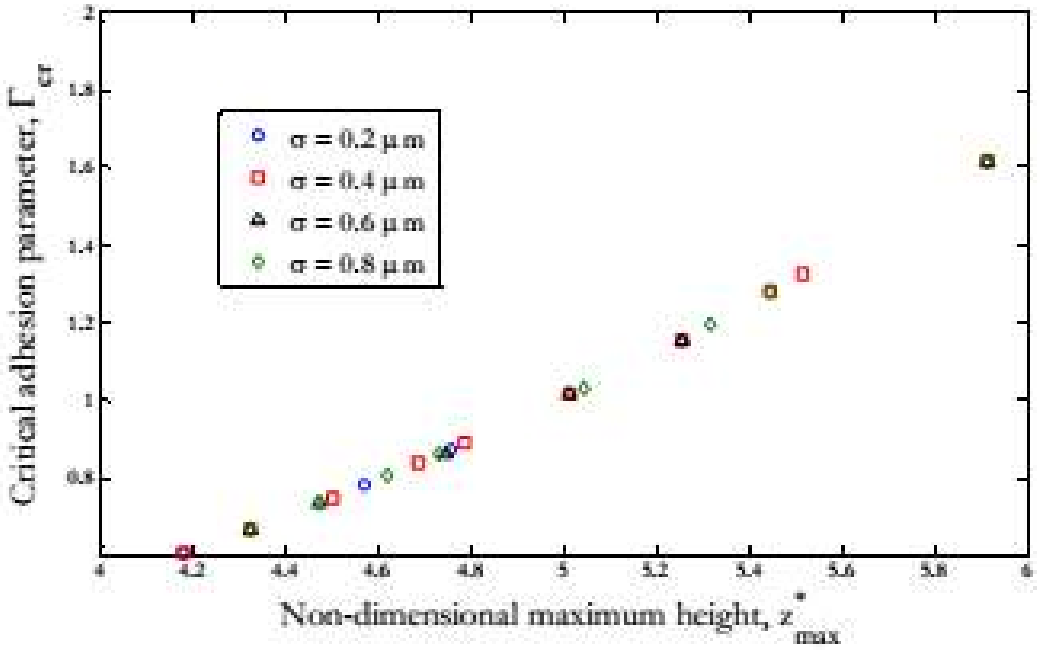

Figure 16. Critical adhesion parameter versus the non-dimensional maximum height for different values of r.m.s. roughness.

Therefore, the critical adhesion parameter, Γ_{cr}, for different Gaussian isotropic rough surfaces is a function of 3 different parameters, non-dimensional liquid volume, V_0^*, non-dimensional external load, P^*, and non-dimensional maximum height, z^*_{max}, i.e.

$$\Gamma_{cr} = f\left(V_0^*, P^*, z^*_{max}\right) \tag{49}$$

In the absence of external load, $P^* = 0$, Γ_{cr} is dependent only on V_0^* and z^*_{max}. An empirical relation is developed for Γ_{cr} based on the extensive results obtained for critical adhesion parameter for different combinations of z^*_{max} and V_0^* (Fig. 17). The relation is given by

$$\Gamma_{cr} = 0.011 z^{*\,2.87}_{max} V_0^{*0.32} \tag{50}$$

The above relation is valid for the non-dimensional liquid volume range, $0.05 < V_0^* < 2$, and non-dimensional surface height range, $4.18 < z^*_{max} < 5.91$[1]. The average relative error

[1] Statistically speaking, depending on the number of nodal points, z^*_{max} will tend to fall within certain bounds. In the current study, we considered 500 surfaces each having 4 million nodal points and the above range represents the total variation observed.

between the empirical Eq. (50) and the numerical results in Fig. 17 is 2.9 %. For cases with $0<\Gamma<\Gamma_{cr}$, the instability does not occur in the interface of contact; when $\Gamma=\Gamma_{cr}$, the interface is at the critical point, and when $\Gamma>\Gamma_{cr}$, the interface experiences instability, and no equilibrium configuration can be found.

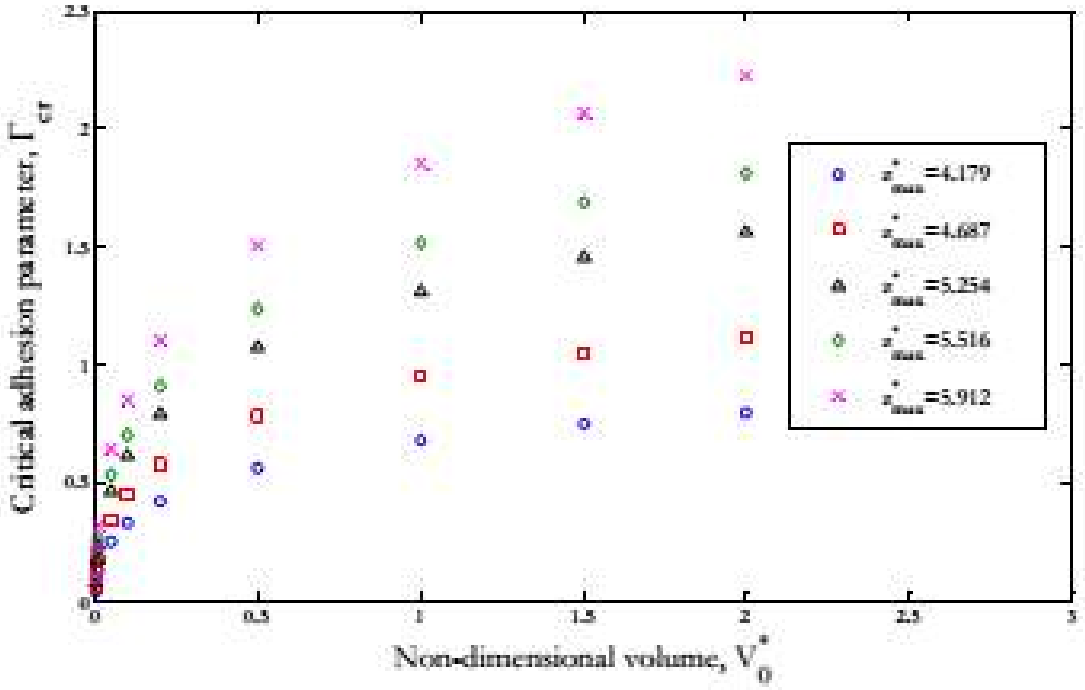

Figure 17. Critical adhesion parameter versus the non-dimensional liquid volumes for different values of non-dimensional maximum surface height.

A 3D plot of Γ_{cr} versus z^*_{max} and V_0^* is shown in Fig. 18. Points above the critical surface represent unstable conditions, while those below are stable.

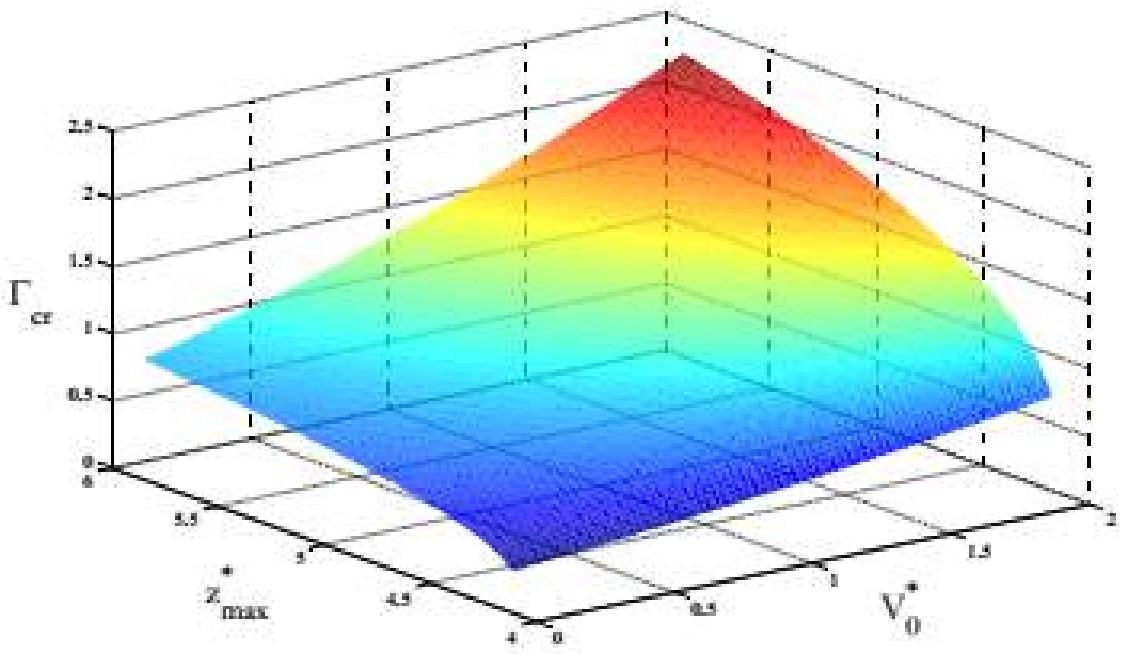

Figure 18. The 3D plot of the critical adhesion parameter versus the non-dimensional liquid volume and non-dimensional maximum surface height for $P^* = 0$

If the liquid volume, V_0, between the rough surfaces is controlled, the following relation can be obtained for the liquid volume which causes instability and is based on the Eq. (50) and substitution for the non-dimensional parameters

$$\frac{\gamma V_0(\cos\theta_A + \cos\theta_B)}{\sqrt{2}\pi A_a^{1/2} E'\sigma^3} = 0.011\left(\frac{z_{max}}{\sigma}\right)^{2.87}\left(\frac{V_0}{A_a\sigma}\right)^{0.32} \quad (51)$$

Simplifying and rearranging Eq. (51), the following relation can be obtained for the critical liquid volume

$$(V_0)_{cr} = 0.012\left(\frac{E'}{\gamma(\cos\theta_A + \cos\theta_B)}\right)^{\frac{1}{0.68}}\left(\frac{z_{max}}{\sigma}\right)^{4.22} A_a^{0.26}\sigma^{3.04} \quad (52)$$

Since the practical range for z^*_{max} is limited, it is better to keep $\frac{z_{max}}{\sigma}$ as one term, and it denotes that z_{max} and σ cannot be chosen completely independently. The above expression highlights the role of certain material properties on the critical volume necessary for interface collapse. It shows that as the roughness of the surfaces increases,

higher value of liquid volume is needed to cause surface instability. Also, it shows for rough surfaces with the same r.m.s. value that as the ratio $\frac{z_{max}}{\sigma}$ increases, the critical liquid volume also increases.

In the presence of external load, P^*, the following relation can be obtained for the critical adhesion parameter, Γ_{cr}, based on extensive number of numerical simulations.

$$\Gamma_{cr} = \frac{1}{\left(8.94V_0^* + 17.15\right) z_{max}^{*\,-1.59V_0^{*0.11}} P^{*0.85}} + \frac{1}{0.011\ V_0^{*0.32} z_{max}^{*\ 2.87}} \qquad (53)$$

where the range $0 < P^* < 5$ is considered for the dimensionless external load, P^*, the range $4.18 < z_{max}^* < 5.91$ is considered for the dimensionless surface height, z_{max}^*, and the range $0.05 < V_0^* < 1.5$ is considered for the dimensionless liquid volume, V_0^*. The average relative error between Eq. (53) and the numerical data is 2.27 %. If the external load, P^*, is set to zero in Eq. (53), it reduces to Eq. (50).

A comparison between the numerically obtained critical adhesion parameter, Γ_{cr}, with the empirical Eq. (53) is shown in Fig. 19. In Fig. 19, the non-dimensional surface height, z_{max}^*, is constant, and the plots for critical adhesion parameter, Γ_{cr}, versus non-dimensional external load, P^*, are obtained for 6 different values of non-dimensional liquid volume, V_0^*.

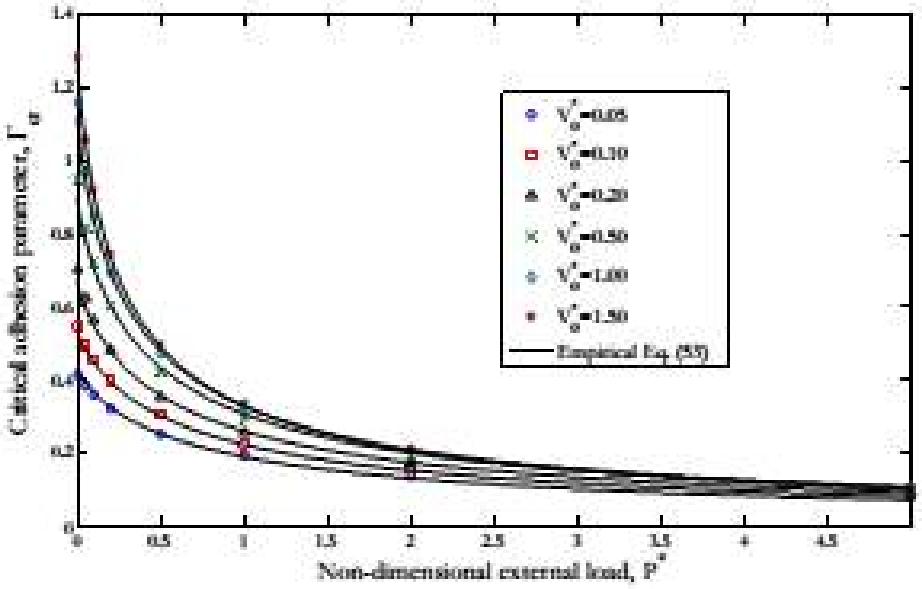

Figure 19. Comparison between critical adhesion parameter results with the Empirical Eq.

4. Conclusions

A numerical model for the liquid-mediated adhesion between 3D, Gaussian, isotropic rough surfaces is developed. The results for the tensile force, average gap, and contact area are obtained and discussed. It is shown that the normalized tensile force increases with the adhesion parameter until the interface reaches a point of instability. Beyond this point, no equilibrium configuration could be found because the compressive force in the contacting surfaces is overwhelmed by the tensile force within the liquid film. This condition is called surface collapse, whereby there is an expected upward jump in the tensile force and wetted radius, as well as a downward jump in the average gap. An empirical relation for the adhesion parameter at the point of instability is obtained based on the material and geometrical properties of the contacting rough surfaces and the liquid film. It is shown that the critical adhesion parameter, Γ_{cr}, depends on the non-dimensional liquid volume, V_0^*, non-dimensional external load, P^*, and the non-dimensional maximum height, z_{max}^* as in

$$\Gamma_{cr} = \frac{1}{\left(8.94V_0^* + 17.15\right) z_{max}^{*\,-1.59V_0^{*0.11}} P^{*0.85}} + \frac{1}{0.011\ V_0^{*0.32} z_{max}^{*\ 2.87}}$$

, which is valid for the range of parameters given below the Eq. (53).

5. Acknowledgements

The authors would like to thank the National Science Foundation (NSF) for support of this work.

References:

(1) Johnson KL, Greenwood JA, Higginson JG. The contact of elastic regular wavy surfaces. International journal of mechanical sciences. 1985;27(6):383-96.
(2) Van Spengen WM, Puers R, De Wolf I. A physical model to predict stiction in MEMS. Journal of micromechanics and microengineering. 2002;12(5):702.
(3) Van Spengen WM, Puers R, De Wolf I. On the physics of stiction and its impact on the reliability of microstructures. Journal of Adhesion Science and Technology. 2003;17(4):563-582.
(4) Komvopoulos K. Adhesion and friction forces in microelectromechanical systems: mechanisms, measurement, surface modification techniques, and adhesion theory. Journal of adhesion science and technology. 2003;17(4):477-517.

[5] Liu H, Bhushan B. Adhesion and friction studies of microelectromechanical systems/nanoelectromechanical systems materials using a novel microtribioapparatus. Journal of Vacuum Science & Technology A. 2003;21(4):1528-1538.
[6] Bhushan B. Adhesion and stiction: mechanisms, measurement techniques, and methods for reduction. Journal of Vacuum Science & Technology B. 2003;21(6):2262-2296.
[7] Lee S-C, Polycarpou AA. Adhesion forces for sub-10 nm flying-height magnetic storage head disk interfaces. Journal of tribology. 2004;126(2):334-341.
[8] Yang SH, Nosonovsky M, Zhang H, Chung K-H. Nanoscale water capillary bridges under deeply negative pressure. Chemical Physics Letters. 2008;451(1):88-92.
[9] Matthewson M, Mamin H. Liquid mediated adhesion of ultra-flat solid surfaces. MRS Proceedings: Cambridge Univ Press; 1988.
[10] Zheng J, Streator JL. A micro-scale liquid bridge between two elastic spheres: Deformation and stability. Tribology Letters. 2003;15(4):453-464.
[11] Zheng J, Streator J. A liquid bridge between two elastic half-spaces: A theoretical study of interface instability. Tribology Letters. 2004;16(1-2):1-9.
[12] Megias-Alguacil D, Gauckler LJ. Capillary forces between two solid spheres linked by a concave liquid bridge: regions of existence and forces mapping. AIChE journal. 2009;55(5):1103-1109.
[13] Matthewson M. Adhesion of spheres by thin liquid films. Philosophical Magazine A. 1988;57(2):207-216.
[14] Poon CY, Bhushan B. Numerical contact and stiction analyses of Gaussian isotropic surfaces for magnetic head slider/disk contact. Wear. 1996;202(1):68-82.
[15] Tian X, Bhushan B. The micro-meniscus effect of a thin liquid film on the static friction of rough surface contact. Journal of Physics D: Applied Physics. 1996;29(1):163.
[16] Streator J. A model of mixed lubrication with capillary effects. Tribology Series. 2002;40:121-128.
[17] Persson B. Capillary adhesion between elastic solids with randomly rough surfaces. Journal of Physics: Condensed Matter. 2008;20(31):315007.
[18] Streator JL, Jackson RL. A model for the liquid-mediated collapse of 2-D rough surfaces. Wear. 2009;267(9):1436-1445.
[19] Streator JL. A model of liquid-mediated adhesion with a 2D rough surface. Tribology International. 2009;42(10):1439-1447.
[20] Rabinovich YI, Adler JJ, Esayanur MS, Ata A, Singh RK, Moudgil BM. Capillary forces between surfaces with nanoscale roughness. Advances in colloid and interface science. 2002;96(1):213-230.
[21] Jackson RL, Streator JL. A multi-scale model for contact between rough surfaces. Wear. 2006;261(11):1337-1347.
[22] Rostami A, Streator JL. A Model for Capillary Flow between Rough Surfaces. STLE Annual Meeting. 2014.
[23] Adamson AW, Gast AP. Physical chemistry of surfaces. 1967.
[24] Rostami A, Jackson RL. Predictions of the average surface separation and stiffness between contacting elastic and elastic-plastic sinusoidal surfaces. Proceedings of the Institution of Mechanical Engineers, Part J: Journal of Engineering Tribology. 2013;227(12):1376-1385.

[25] Green CK, Streator JL, Haynes C, Lara-Curzio E. A Computational Leakage Model for Solid Oxide Fuel Cell Compressive Seals. Journal of fuel cell science and technology. 2011;8(4):041003.
[26] Johnson KL, Johnson KL. Contact mechanics: Cambridge university press; 1987.
[27] Whitehouse DJ, Archard J. The properties of random surfaces of significance in their contact. Proceedings of the Royal Society of London A Mathematical and Physical Sciences. 1970;316(1524):97-121.
[28] Garcia N, Stoll E. Monte Carlo calculation for electromagnetic-wave scattering from random rough surfaces. Physical review letters. 1984;52(20):1798.

7th International Conference on Tribology in Manufacturing Processes

การประชุมวิชาการนานาชาติด้านไทรโบโลยีในกระบวนการผลิตครั้ง ที่ 7

Written by Asst.Prof. Numpon Mahayotsanun (Khon Kaen University)

INTRODUCTION

International Research Group of Tribology in Manufacturing (IRGTM) in collaborations with Thai Tribology Association (TTA), National Metal and Materials Technology Center (MTEC), King Mongkut's University of Technology Thonburi (KMUTT), and Khon Kaen University (KKU) are organizing the 7th International Conference on Tribology in Manufacturing Processes (ICTMP) during February 28 to March 2, 2016 in Phuket, Thailand.

The aim of the conference is to present the latest developments in the research of tribological aspects in manufacturing processes, particularly in the following topics:

- Tribology in forming processes
- Tribology in cutting and finishing processes
- Tribology in joining processes
- Functional surfaces
- Advanced (nano/bio) tribology

The scope of interest is related to friction, lubrication, wear, surface engineering, process modelling, applied plasticity and environmental issues. In this conference, we are strongly interested in **"Tribology of Tool Materials and Designs for High Performance and Extended Service Life"**. Focused tool applications are (but not limited to):

- Extrusion
- Forging
- Machining
- Stamping

The applications can range from nano scale, to micro/meso scale, to macro scale. In addition, the presentations include practical guidelines for solving tribological problems in an industrial environment.

The conference will be held at Mövenpick Resort & Spa Karon Beach Phuket, Thailand from Sunday February 28 to Wednesday March 2, 2016. Please note that all the accepted articles will be published in the **Proceedings of ICTMP 2016 (ISBN: 978-616-92565-0-2)**.

KEYNOTE SPEAKER

Prof. Peter Groche
Technische Universität Darmstadt
Germany

KEYNOTE SPEAKER

Prof. Yoshinari Tsuchiya
Gifu University Composite Materials Center
Japan

KEYNOTE SPEAKER

Prof. Tatsuhiko Aizawa
Shibaura Institute of Technology
Japan

KEYNOTE SPEAKER

Assoc.Prof. Gracious Ngaile
North Carolina State University
USA

KEYNOTE SPEAKERS

Prof. Kuniaki Dohda
Northwestern University
USA

INDUSTRIAL PRESENTATION SPEAKER

Mr. Masato Otake
Nihon Parkerizing Co., LTD.
Japan

INDUSTRIAL PRESENTATION SPEAKER

Mr. Nutthawut Rungsimutuchat
PTT Public Company Limited
Thailand

INDUSTRIAL PRESENTATION SPEAKER

Dr. Eric Gard
InS France, InS Thai, EMTT, Crealins
France, Thailand

INDUSTRIAL PRESENTATION SPEAKER

Dr. Yoshikatsu Nagasawa
Analytical Chemistry
Japan

INDUSTRIAL PRESENTATION SPEAKER

Dr. Wanxin Sun
Bruker Nano-Surface
Singapore

INFORMATION

For more information regarding ICTMP 2016, please visit www.ictmp2016.com. You can also contact

Thai Tribology Association (TTA)
131 Thailand Science Park,
INC 1 Bldg., Room 234
Phahonyothin Road, Khlong Nueng
Khlonh Luang, Pathumthani 12120 Thailand
Tel. +66-2564-7200 ext. 5234
Mobile. +66-94-698-8322
Email. admin@ictmp2016.com

Machine Reliability Through Excellent Lubrication Pratices in MHE'16

การสร้างความเชื่อถือของเครื่องจักรผ่านการประยุกต์ใช้การปฏิบัติด้านการหล่อลื่นอย่างเป็นเลิศ ในงาน MHE'16

Written by Vichai Srimongkolkul
Email. usa@oilpure.com
Tel. 080-652-2553

HIGHLIGHTS

"A World-Class Manufacturing Training Series to Fundamentally Manage Equipment & Asset for Profits". This is a ane day course workshop co-sponsored with MTEC and Thai Tribology Association (TTA), which will be held on March 27, 2016 during 9.00-16.00 at Impact Muangthong Thani as part of the Material Handling & Machinery Exhibition 2016 (MHE'16).

INTRODUCTION

Best practice of excellence lubrication to improve plant equipment and its reliability will lead company to a more profitable operation. Reliability management can be controlled by excellence lubrication practices which will improve company return on asset, thus lead to enhance shareholder value and earning from better corporate return on investments. This hidden cost occurs from the fact that 80% of equipment root cause failure comes from lubrication failure. Today business rules have changed. Corporate hidden profit can be obtained within the company by improving machinery productivity and cost savings. Every internal productivity cost savings is easier to access for profit than the profit that comes from sales revenue deducted the operating costs.

YOU WILL LEARN HOW TO

- Basic lubrication course, understanding oil additives and its base oil properties.
- How to design lubrication program for plant machinery applications.
- Basic oil filtration technology & effective oil contamination control.
- How to establish used oil analysis program that solves machinery problems.
- How to read oil analysis and interpretation oil property analysis.
- An operating plan to reach the Zero Down Time operation with TPM (Total Productive Maintenance) that works for Thai culture.
- Root cause analysis and Proactive Preventative Oil Maintenance Program.
- A newly evolved TPR (Total Process Reliability) that is replacing TPM.

MATERIAL HANDLING & MACHINERY EXHIBITION 2016

งานมหกรรมแสดงเครื่องจักร เพื่อการขนส่งลำเลียง และการจัดเก็บ ครั้งที่ 2

"ลดต้นทุนเพิ่มผลกำไร ตอบโจทย์รับ AEC"

พบกับสินค้าอุตสาหกรรม ลดสูงสุด 30%-70%

**ภายในงานเท่านั้น

สอบถามข้อมูลเพิ่มเติม./จองบูธ
Tel: 086-399-8080
E-mail: mheexhibition@gmail.com
www.mheexhibitions.com

25-28 March 2016

Hall 6 Impact Muang Thong Thani

Supported By:

Officially Supported By:

Organizer by:

ใบตอบรับ กรุณาแฟกซ์เอกสารกลับมาที่ 02-197-8364 **เพื่อรับของพรีเมี่ยม และส่วนลดค่าพื้นที่งานแสดงสินค้า

มีความสนใจที่จะ: ○ เข้าร่วมแสดงสินค้า พื้นที่ขนาด _____ ตร.ม. ○ สนใจเข้าร่วมเป็นผู้สนับสนุนหลักของงาน
○ สนใจเข้าร่วมชมงาน ○ ต้องการข้อมูลเพิ่มเติม ○ กรุณาติดต่อกลับ

ชื่อ-นามสกุล: _____ ตำแหน่ง: _____
บริษัท: _____ ที่อยู่: _____
รหัสไปรษณีย์: _____ โทรศัพท์: _____ โทรสาร: _____ อีเมล์: _____
เว็บไซต์: _____ ประเภทของสินค้าและธุรกิจ: _____

WHY ATTEND THIS TRAINING?

- Transform your business to become World-Class Manufacturing.
- Learn to discover the new hidden costs by improving
- Learn to become a Lubrication Excellence for your operation.

WHO SHOULD ATTEND

- Lubrication engineer
- TPM manager
- Maintenance professionals
- Plant Managers
- Reliability Managers and Engineers
- Operation manager
- Production Manager and Directors
- Lubrication Sales Professionals

MACHINE RELIABILITY OUTLINE

- How lubrication affect Machine Reliability
- Lubrication fundamental
- Used oil analysis and test result interpretation FT-IR Infra-Red scan, ICP etc.
- Oil Contamination Control
- Oil additive & base oil function for better lubrication.
- Secrets of successful TPM (Total Productive Maintenance) program
- Selecting lubrication for different machinery applications
- Financial benefits from achieving lubrication excellence
- Cost reductions in maintenance and operation
- Asset utilization
- Oil management system
- US Best practices of case studies in paper mills, petroleum plant, plastic injection molder
- Lessons learned from BP oil spill from Machine reliability & lubrication practices
- Lessons learned from BP oil spill from Machine reliability & lubrication practices

SPEAKER

Vichai Srimongkolkul
President, OilPure Technologies, Inc.
Kansas City • Missouri • USA

OILPURE SYSTEMS
The Machine Reliability Company

In 2004, Vichai was selected by US government under Bush's administration to receive a study grant affiliating with Missouri Enterprise (www.missourienterprise.org) to become an Advanced

Manufacturing Specialist from University of Missouri, Rolla school of Engineering. He became a certified specialist in Black Belt Six Sigma, Lean Manufacturing, Supply Chain Management, Baldrige National Quality Program, and ISO 9001-2000 Certification.

During his last 30 years in America, he applies this knowledge to help American industries to improve productivity and adapt their manufacturing process into the 21st century world-class manufacturing. Example of his US clients are Ford Motor, Honda American Motor, Toyota USA, Inland Paper, International Paper, US Navy for nuclear submarine, Israel Electric Co., and etc. Some of his work becomes Best Practice and Benchmarking of the companies. He has written many technical articles for industrial magazines and lectures seminars in lubrication engineering and tribology, beside the area of World-Class Manufacturing, Total Productive Maintenance (TPM), Design of Experiments (DOE), Machine Reliability Center, industrial automation, Zero downtime operation, quality control in oil contamination as related to Statistical Process Control (SPC), and in-house oil recycling programs etc. In 2007, Vichai was invited by Columbian government in South America to work on the new development of biodiesel technology that can be appropriated for Columbia municipal government. In 1988, Vichai joined CLARCOR, Inc. (www.clarcor.com), a billion dollar in sales company, which located in Rockford, Illinois as general development manager in research & development in filtration. After the second year of his employment, he became one of the top 30 key executives who helped manage CLARCOR business.

Vichai developed a new oil purification technology, OilPure process for American industries since 1988. Most of his US customers has extended their lubricant life and the same oil has been in service up to 10 years. These customers dramatically reduce the need to buy new replacement oil, reduce the cost of waste oil disposal and increase machine reliability performance. During his R&D development, he invented OilPure technology which was patented in 1992 under his name — US patent no. 5,112,479. OilPure Systems has won the 1989 Gold Award Product of the Year from Plant Engineering publication during its development. During that time he becomes a member of ASTM technical committee, D-2 for lubrication and D-15 for engine coolant, who helps develop lubrication and coolant specifications.

BP OIL SPILL AT THE GULF

As part of supply chain for BP Oil with Veolia Environmental Services, Vichai from OilPure Technologies, Inc., helps establish the oil management to support Veolia's Robot Submarine hydraulic oil and recycle their lubrication in the vessel during the oil spill.

INFORMATION

Please call 094-698-8322 to register for the training.

HONDA

Honda R&D Asia Pacific Co., Ltd.

HONDA
Honda R&D Asia Pacific Co., Ltd.

THAI
TRIBOLOGY
ASSOCIATION
สมาคมการสึกหรอและการหล่อลื่นไทย

Thai Tribology Association (TTA)
131 Thailand Science Park, INC 1 Bldg., Room 234, Phahonyothin Road, Khlong Nueng, Khlonh Luang, Pathumthani 12120 Thailand
Website: www.tta.or.th | Email: admin@tta.or.th